VECTOR VELOCITY FLUCTUATIONS OF PROPAGATING STALL IN AXIAL FLOW COMPRESSORS

Thesis by

Charles A. Bodeen

First Lieutenant
United States Air Force

In Partial Fulfillment of the Requirements

For the Degree of

Mechanical Engineer

California Institute of Technology

Pasadena, California

1961

ACKNOWLEDGMENTS

Professor W. D. Rannie was invaluable for his suggestions, guidance, and evaluation of this research.

Professor E. E. Zukoski provided stimulating discussions of the research techniques.

Mr. F. Tyler Linton is, to a large degree, responsible for the success of the research because of his extremely high competence as machinist, research assistant, instrument builder, data reductionist, draftsman, and historian of past research techniques, both successful and unsuccessful. It would be impossible to estimate the time saved because of his ability and experience.

Mrs. Roberta Duffy was very helpful in the preparation of the manuscript, and Mrs. Beverly McAllister provided much needed assistance in the early phases of data reduction.

The Institute of Technology, Air University, United States Air Force was responsible for me financially. Col. B. P. Blasingame, formerly Professor of Astronautics, USAF Academy, selected me for the program. Col. Richard C. Gibson, Professor of Astronautics, USAF Academy, offered valuable and continuing advice on both my military and academic careers.

The equipment used for this research was provided by the United States Navy under contract Nonr-220(23).

ABSTRACT

The angular velocity of propagation of a single cell partial span propagating stall traveling on an isolated, or relatively isolated, axial compressor blade row was found experimentally to be equal to the downstream angular velocity of the flow outside the stall cell between successive passages of the stall cell averaged over the blade span. In a machine consisting of three identical stages, a similar stall was found to propagate at the mean of two such averages, i.e., upstream and downstream from any interior blade row. The sides of partial span stall cells were found to be streamtubes in several cases.

Other general but less significant observations of propagating stall are reported. The hot wire anemometers used to measure unsteady vector velocities are described.

TABLE OF CONTENTS

SECTION	TITLE	PAGE
	Acknowledgments	
	Abstract	
	Table of Contents	
	Symbols	
I.	INTRODUCTION	1
II.	TEST EQUIPMENT	5
	2.1 Axial Flow Compressor and Standard Instrumentation	5
	2.2 Hot-Wire Anemometry	6
	2.2.1 Circuit	7
	2.2.2 Angular Behavior of Hot Wires	8
	2.2.3 Hot-Wire Probes	9
III.	EXPERIMENTAL RESULTS	15
	3.1 General Characteristics of Stall	15
	3.1.1 Throughflow	15
	3.1.2 Spiraling	17
	3.1.3 Full Stall Transition Zones	18
	3.2 Vector Velocities	20
	3.2.1 Tangential Flow	20
	3.2.2 Radial Flow	22
IV.	DISCUSSION OF EXPERIMENTS	24
	References	30
	Tables	33
	Figures	35

SYMBOLS

A	area of compressor annulus
a	fraction of annulus supporting reversed flow
b	fraction of annulus supporting transition flow
c_1, c_2	constants in King's Equation (Sec. 2:2.1)
c	component of flow velocity
Δc_u	$c_{u_1} - c_{u_2}$
R	hot wire resistance
R_a	hot wire resistance at ambient air temperature
r_u	radial coordinate
v	flow speed
v_i	flow speed indicated by hot wire
v_1, v_2	flow speed indicated by hot wire 1, 2.
α	angle between flow velocity and bisector of angle between wires of "V" probe
β	flow angle measured from plane of blade row in coordinate system moving with rotors
γ	flow angle measured from plane of blade row in coordinate system fixed to stators
δ	half-angle between wires of "V" probe
θ	angle between flow velocity and normal to hot wire
λ	$\Delta c_u / u_o$
ξ	r/r_o -- dimensionless radius
ρ	density of air
τ	dimensionless torque
ϕ	c_a/u_o -- local flow coefficient

ω c_u/r -- flow angular velocity

ω_s angular velocity of stall

ω_o u_o/r_o -- rotor angular velocity

Subscripts

a axial

n unstalled flow between stall cells

o tip

s stall cell

t transition zone

1 just upstream from rotor

2 just downstream from rotor

Averaging Processes:

For $f = r, \xi, \omega$

$$\bar{f} = \frac{\int_{.6}^{1} f \, d\xi}{\int_{.6}^{1} d\xi}$$

For $f = \phi$

$$\bar{f} = \frac{\int_A \phi \, dA}{\int_A dA}$$

I. INTRODUCTION

When the angle of incidence on a blade row of an axial compressor is increased due to off-design operation caused by starting, acceleration, or reduced flow in throttling, the individual blades stall, much the same as isolated airfoils. The blades rarely stall over the entire annulus; the preferred mode is for a group (or groups) of blades to stall, and for the pattern of stalled flow to be propagated, unchanged in shape, around the blade row. A simplified scheme of stall propagation on a two-dimensional cascade is shown in Figure 1. The air incident on the stalled blade row is deflected so that the angle of attack is increased on one side of the stall cell, and decreased on the other side; thus the area of stalled flow propagates.

There are two compelling reasons for interest in propagating stall. First, stall occurs at flow rates very near those of maximum efficiency and sometimes results in an abrupt lowering of compressor performance. Thus, stall is an ever-present hazard in virtually every compressor application. Second, since the blades lose a considerable fraction of their lift as the stall cell passes, propagating stall represents a periodic forcing function on them. Numerous cases of compressor destruction caused by the fact of coincidence of stall propagation frequency with the natural frequency of the blades have been reported.

Stall was first discovered in the development of the British jet engines in 1945 (2), while its propagating nature seems to have been reported first in 1950 (16).* Since that time, there have been many in-

* Reference (16) was classified at the time of its publication. In the unclassified literature, stall propagation was discovered independently and almost simultaneously by three groups of investigators about 1951 ((3), (4), (5)).

vestigations of the phenomenon in a variety of machines (e.g. (1), (3), (4), (5), (9), (10), (11), and (17) through (24)). The diversity of the observed stall characteristics is amplified by the fact that most machines exhibit several stalling modes over different ranges of flow rates. The results of these studies of different machines and of systematic changes in the blading of any particular machine have produced results which are so complex and varied that it is difficult to derive from them statements of general validity. A few of the outstanding characteristics are as follows:

1. Most of the stalls reported involve large, rather than small perturbations from the mean flow. Low amplitude stall of a type consistent with linearized theories (see below) has been found in a rectangular cascade and in an annular cascade (9).

2. The stall disturbances may be concentrated near the hub or near the case in low hub ratio machines, but usually extend more or less evenly over the entire blade span in compressors of high hub ratio and in low hub ratio machines at very low flow rates. Because of the relative amount of the span involved, the concentrated stalls have been termed <u>partial stall</u>, and the others <u>full stall</u>. A third basic type of stall involving disturbances at both the hub and the case which are out of phase with each other was discovered in the course of the research for this paper, although it was not studied in detail.

3. Stalls usually start as one patch or <u>cell</u>. As the flow rate is decreased, the size of this cell increases to a point and then

the cell splits, forming two approximately diametrically opposed cells. In some machines, this splitting may produce as many as 12 distinguishable cells. In others, the single cell pattern may not be found and/or the number of cells may decrease as the flow rate is reduced (e. g. (10), (11)).

4. Each partial stall cell usually involves not more than 20% of the annular area, while full stall cells may occupy more than 60% of the annular area.

5. In a stationary system, the rotative speed of the stall is always less than that of the rotor and in the same direction. In general, the propagation speed becomes lower as the flow rate is decreased.

6. The stalling characteristics of a blade row are markedly affected by the close proximity of other blade rows.

Theories of stall propagation soon followed the experimental investigations. Several approaches to the linearized problem of a small disturbance propagating along a single two-dimensional blade row have been developed ((3), (6), (7), (8)). A non-linear theory involving the shedding of discrete vortices (17) and a restricted solution to a three-dimensional theory (18) show the beginnings of a more realistic approach to the problem from the theoretical point of view. Some of the theories have been able, by the suitable adjustment of undetermined parameters, to predict or "explain" stall propagation velocities within 10 -20% . Others give rough indications of the conditions necessary

for the initiation of propagating disturbances, but none can predict the number of stall cells, their annular extent, or the magnitude of the velocity disturbance, all of which are important in the consideration of possible blade failure.

The development of adequate theories has suffered from a lack of generally applicable experimental data, and the experiments have suffered, for the most part, from a lack of adequate instrumentation to deal with the complex unsteady flow fields of propagating stall. For this reason, the work described in this paper has been directed toward practical application of hot wire anemometry to the stall problem and toward a search for further descriptive statements which may be applicable to a majority of cases of propagating stall. Although a wide variety of compressor configurations were studied, the goal was not a detailed description of each type of stall pattern, but rather the discovery of any unifying trait which might be characteristic of all propagating stalls.

II. TEST EQUIPMENT

2.1 Axial Flow Compressor and Standard Instrumentation

The compressor shown in Figures 2 and 3 is the same one which was used for the studies of stall propagation reported in references (5) and (9). The machine and the instruments described in this section are treated in more detail in references (12) and (13).

The compressor hub ratio is 0.6 and the tip radius is 18 inches. The machine is driven by a 125 horsepower dynamometer on a shaft which passes through the vertical exit duct. A honeycomb screen placed in the bell-mouthed cylindrical entrance duct provides flow at the pre-rotation or entrance guide vanes in which turbulence is low enough for accurate calibration of hot wire anemometers. An electric motor with a high gear ratio drive unit permits precise control of the opening of the two rectangular doors which comprise the throttle at the upper end of the exit duct.

Each blade of the three-stage compressor is separately removable, making possible a wide range of compressor configurations. The maximum solidity (nominally unity) was used throughout these tests, there being 30 rotor blades and 32 stator blades per row. There are available three identical stages of free-vortex blading and one stage of solid-body blading. Root, tip, and mid-radius sections of the blades are shown in Figure 4, and their geometric properties are presented in Table I.

The flow rate through the compressor had been previously calibrated as a function of the inlet duct wall pressure, and this pressure was read from a movable-well water manometer.

Instrument ports are located at various tangential positions aft of each blade row and in front of the entrance guide vanes as shown in Figure 5.

Steady velocities, used in calibrating the hot-wire anemometers, were measured with a standard pitot static tube coupled with an electric pressure transducer in conjunction with a bridge network and a Brown precision indicator. This system measured the velocity head within about 1% . The directions of the steady velocities (used mostly to calibrate hot-wire anemometers) were measured with a claw-type yaw probe to within 1/2 degree.

A radial survey carriage, shown in Figure 6, was used to position the pressure-sensitive probes and the hot-wire anemometers. The radial position of a probe in this carriage can be set with a least reading of 0.01 inches, while the angular position can be set with a least reading of 0.1 degree.

The rotational speed of the machine was measured by using a coupled counter and timer in conjunction with a small synchronous generator which is directly coupled to the dynamometer shaft. A period of one minute was used to determine the speed with an accuracy better than 1/2 rpm. All studies of stall were made at speeds between 500 and 750 rpm after it was determined that the character of stalling at the maximum speed of 1500 rpm was not significantly different from that at the lower speeds.

2.2 Hot-Wire Anemometry

Unsteady velocities within and between the stall cells were

measured with several types of hot-wire anemometers. References (14) and (15) contain quite complete discussions of the theory of the hot-wire and offer helpful suggestions for the construction of probes for the measurement of vector velocities.

2.2.1 Circuit. The constant current hot-wire circuit which was used throughout the investigation is shown in Figure 7. The 90-volt batteries, each made up of 45 2-volt cells, and the regulating resistors, were chosen with power ratings far in excess of that required to heat the hot-wires so that these elements would not contribute to hot-wire calibration drift. A selector switch on each side of the circuit permitted the use of several anemometers in the machine at one time. This feature was especially convenient when the qualitative nature of propagating stall was being observed, because it was possible to check stall characteristics at different radii and on different survey planes almost simultaneously. The 2-volt variable ground bias permitted the use of higher gain in the oscilloscope, as it was then necessary to amplify only the difference between the instantaneous hot-wire voltage and the mean value to which the bias was set.

In operation, the current regulating resistance used was about 900 ohms, while the resistance of the platinum hot-wires, which were 0.0004-inch diameter and 3/16-inch long, varied(with velocity changes) between 8 and 10 ohms. The nominal current, then, was 100 milliamperes, and it was constant within 2%. With this 2% error, the assumption of constant current produces an error of about 3% in velocities calculated on the basis of King's equation.

$$\frac{i^2 R}{R-R_a} = c_1 + c_2 \sqrt{v} \quad .$$

Errors of about the same magnitude are produced by the general tendency of the hot-wire calibration curves to drift with use. The general calibration procedure was to record, before and after a run, the voltage across the hot-wire as a function of the velocity head at the point in the entrance vane channel used for calibration. Interpolation between calibration points was made graphically, so that the error inherent in the assumption of constant current was eliminated. Calibration flow speeds were measured with a pitot static tube at the same relative position as that of the hot wire, but in the adjacent blade channel.

The frequency response of the oscilloscope amplifiers is flat to 10 kc. Using the methods of reference (14), the response of the hot-wire was estimated to be adequate to 400 cps. At 600 rpm the blade wakes cross the wire at 300 cps; a three-cell stall pattern traveling at 70% rotor speed corresponds to 21 cps.

2. 2. 2 Angular Behavior of Hot Wires. Hot-wire anemometers are relatively less sensitive to flow parallel to the wire than they are to flow normal to it. In fact, over a limited range of angles, θ, between the incident flow and the normal to the wire, the wire behaves as if the flow were normal and of magnitude $v_i = v \cos \theta$, as is shown in Figure 8.

Measurements of radial components of velocity during stall have indicated that the flow between the stall cells is essentially two dimensional. Thus, by using two wires placed at different angles on the same probe, it is possible to make simultaneous measurements of

both speed and direction of the flow. Similarly, a single wire, properly oriented, can be used to read roughly the axial component of velocity alone or the tangential component alone.

2.2.3. Hot-Wire Probes. All of the probes used could be mounted in the instrument carriage shown in Figure 6. In addition, simple survey port plugs, drilled to accommodate the probes, were used to position the instruments for qualitative measurements.

Single wire probes, shown in Figure 9, were used to make preliminary determinations of the velocity fluctuations of the stalled flow and to observe its qualitative nature. In two-dimensional flow, the probe with the wire perpendicular to the axis of the probe support is suitable for measurements of tangential or axial components of velocity and is sensitive to changes in the flow angle. The probe with the wire parallel to the support axis measures the magnitude of the velocity and is insensitive to purely angular disturbances. Either of these probes can be used to determine the stall propagation speed in conjunction with a timing signal, and the phase shift between the signals from two tangentially displaced probes determines the number of cells in the stall pattern.

The two wires which form the V of the probe shown in Figure 10 lie in a plane which is perpendicular to the axis of the probe support. Restricting the discussion to the two-dimensional flow depicted in Figure 10, and assuming that δ is sufficiently large and α sufficiently small for the cosine law to hold,

$$v_1 = v \sin(\delta - \alpha)$$

$$v_2 = v \sin(\delta + \alpha)$$

These equations yield

$$\alpha = \tan^{-1}\left(\frac{v_2 - v_1}{v_2 + v_1}\tan\delta\right),$$

and v may be computed from either of the original equations after α is known. As may be seen from Figure 8, high sensitivity to angular disturbances requires small δ, whereas agreement with the cosine law requires large δ. At reduced speeds encountered within the cells, the cosine law is followed only as $\delta \longrightarrow 90^{\circ}$. Since the purpose of the study at the time the V-probe was built was an investigation of conditions between the cells, δ was chosen as 30°. With the use of an optical comparator, the relationship between the characteristic direction of the V and the instrument carriage angle dial could be determined within 1/4 degree.

In use, the probe was aligned in the machine so that the mean velocities between the stall cells were nearly equal. This made $\alpha \approx 0^{\circ}$ so that variations in the flow angle of $\pm 10^{\circ}$ at the between-stall speed did not take the wire far off the cosine curve. At low speeds, the assumption of the cosine behavior where it is not warranted leads to measured speeds being higher than actual speeds, and measured angular deflections lower than the actual deflections.

The L-probe shown in Figure 11 consists of one wire mounted parallel to the axis of the probe support, and one perpendicular to it. Again restricting the discussion to two-dimensional flow in a plane perpendicular to the probe support, it will be seen that the wire parallel to the probe axis is sensitive only to the magnitude of the flow velocity. If

the other wire is aligned so that the mean flow makes an angle of 45° to 60° with the normal to the wire, the indicated velocity will be a sensitive function of both the speed and the direction of the flow.

In practice, both wires of the L-probe were calibrated simultaneously in flow normal to the plane of the wires. Then the instrument carriage was installed at a selected survey plane, and the carriage angle was fixed at a value which made the mean flow incident on the angle-sensing wire at about $\theta = 50^{\circ}$. A stall study run would be made which did not exceed 30 minutes in length. During the run, several photographs of the wire signals were made at a number of radial positions, using a Polaroid camera. These photographs were quickly studied, and a "typical" or "mean" example of the stall pattern at each radius was selected for data reduction.

On the photographs which were selected, the oscilloscope readings for both wires were recorded for several "significant" points. The coordinate of each point was normalized against the pattern wave length. Blade wake disturbances were averaged out of the readings by eye. Next, the probe was returned to the calibration position in the entrance guide vane row. The direction of the flow at this position had been measured previously and was found to be nearly independent of the flow speed, with a maximum angular variation with speed of about 1/2 degree. During the angular calibration which followed, the flow was assumed to be in a constant direction.

The angular calibration consisted of serially matching the flow conditions on the L-probe with the flow conditions which produced the

hot-wire signals of the selected data points. First, the speed of the incident air was adjusted by changing the rotative speed of the machine or adjusting the throttle. The speed could be matched quite easily just by matching the voltage on the wire parallel to the probe axis with the voltage on the same wire which was recorded for the data point in question. Next, the instrument carriage was turned until the voltage across the angularly sensitive wire matched that for the data point. Finally, after all data points were calibrated for speed and angle, both wires were given a normal-incidence calibration. If the calibration curves of either wire differed by more than 3% from the pre-run calibrations, the data was not used.

This method of calibration was not too laborious, for the data points were selected only where the time rate of change of the slope of the signal was large. There were usually several points in each run which had very nearly the same velocity, the angles of which could be read without changing the flow rate. Likewise, the system was not as crude as it might seem, because the vector velocities of the data points easily could be reproduced within the natural variations from one stall cell to the next in the same rotating pattern or between successive passes of the same cell. These variations were roughly 3% on speed and $1\frac{1}{2}^{\circ}$ on the flow angle. An example of an oscilloscope photograph, the selection of data points, and the reduced data are shown in Figure 18. It should be pointed out that this technique of calibration is not practical for V-probes because in that case both wires are sensitive to speed and angle, which makes matching almost impossible. It was not necessary to use the optical comparator with the L-probe, since the

difference between the absolute flow angle of the data point and known flow angle at the calibration point was measured directly.

The radial V-probe shown in Figure 12 was used to measure the radial component of the flow. In use, the probe was aligned so that the plane of the two wires contained the mean flow vector between the stall cells. It is easily shown that excursions of this vector of up to 20° out of this plane produce a maximum error of 10% in the measured radial component of the flow and 2° in the measured angular deviation of the flow from a tangential plane. Excursions of 20° were about the maximum found in partial span stalls.

The wake from the leading wire of the radial V-probe made it difficult to obtain precise quantitative data concerning radial flows, so those data are presented only qualitatively in this paper.

In full stall regimes, reversed flow within the stall cell was easily detected by observing the deflections of a tuft on the end of a rod inserted into a radial survey port. In order to correlate the reversal of flow with the other hot-wire measurements, the reversal indicator shown in Figure 13 was designed. The probe consisted of two parallel hot wires, separated by a porous shield made of fine screen and stuffed with steel wool. A variety of solid and porous separation shields was tried before the desired angular behavior (Figure 14a) was closely approximated (Figure 14b). When the qualitative behavior of the flow speed was simultaneously obtained from a single radial hot wire, it was very easy to detect flow reversal using the scheme presented in Figure 14c. The increased turbulence of the signal from the leeward wire also helped to discern reversal.

As can be seen from the angular behavior of the signals from

the two wires, if the flow was normally incident on wire A in the unstalled or between stall conditions, a change in direction of 120° to 240° was clearly identifiable as a reversal. Reversed flow is that flow which has a negative axial component of velocity. Considering the flow angles usually found in axial compressors, changes in flow angle larger than 240° might be encountered in reversed flow. By aligning the flow reversal probe so that the unstalled flow is incident at -60° from the normal, angular changes up to 300° can be detected.

Some investigators have reported that since the speed indicated by a single hot-wire anemometer failed to pass through zero, there was, necessarily, no reversed flow involved in the propagating stalls they studied. It should be noted that a vector velocity can be reversed without experiencing zero magnitude. Furthermore, the reversal of flow need not involve direction changes of 180°. It was for these reasons that the flow reversal probe was designed to have the characteristic angular behavior shown in Figure 14.

III. EXPERIMENTAL RESULTS

3.1 General Character of Stalls

3.1.1 Throughflow. The V-probe and the flow reversal probe were used to determine the general nature of both partial and full span propagating stalls. While the signal from the V-probe was very difficult to interpret within the stall cell, vector velocities (assuming radial flow to be negligible) were easily measured in the flow area between cells. In the three-stage free-vortex machine, these velocities were found to be quite close to the velocities found in unstalled flow with stall imminent. In the single-stage free-vortex and solid-body machines, similar results were found.

From the vector velocities, axial speeds were determined, and the flow rate outside the stall cell was integrated. Eleven radial positions were used for these measurements. Simultaneously, the entrance duct wall pressure was measured and from it, using a previous overall flow rate calibration, the total flow rate was determined. The difference between the total flow rate and the flow rate measured between the stall cells was taken to be the flow rate within the cells.

For three-stage free-vortex blading, it was found that within a single cell partial span stall, the average local flow coefficient is positive and of magnitude $\phi_s = 0.70\,\overline{\phi}$. This means that 23% of the total flow passed through the 33% of the area of the annulus which was occupied by the stall cell.

Similar measurements for a full span stall in the three-stage machine indicated the presence of reversed flow, since it was found that $\phi_s = -0.11 + 0.60\,\overline{\phi}$.

The flow reversal probe was applied to both of the previously mentioned stalls. A qualitative picture of the distribution of axial velocities for full and partial span stalls in the three-stage free-vortex machine is presented in Figure 15. In the figure, a "+" indicates flow in the normal direction, and a "-" indicates reversed axial flow. The proximity of neighboring symbols is indicative of the relative magnitude of the axial component of velocity. The portions of the flow which show significant departures from the pre-stall condition are called the "stall cell" and are outlined. These qualitative pictures are typical of flow just downstream from any of the three rotors. The flow downstream from the stators differed somewhat as is evidenced by Figure 23 which is discussed later. Flow ahead of the first rotor took on the "softened" look of a potential disturbance in all cases.

The hub boundary layer in partial stall is shown as entirely reversed, although this may not be the true situation. The boundary layer is, of course, very turbulent and the flow reversal probe did indicate reversed flow, but the reversed flow could easily have been mixed with forward flow within any single blade channel.

The full stall exhibited clearly defined reversed flow over most of the stalled area, with areas of increased axial velocity forming "transition zones" on the leading and trailing edges of the stall. The area across the greater portion of the interior of the full stall cell was found to consist of almost constant velocity flow at any radius. Rough measurements were made at mid-radius of the entire flow field through all three stages in and close to the full stall cell. The velocities found are shown relative to the stall cell in Figure 16. The length of the flow

arrows in the figure indicates the magnitude of the velocity normalized against the local absolute rotor speed.

3.1.2 Spiraling. Two single wire anemometers were used to determine whether the stall cell extended straight back through the machine parallel to the axis, or if it spiraled. Survey planes 2, 4, 6, and 8 were used for this study. One anemometer was fixed in one of the selected planes, and the other was placed alternately in each of the other three to determine the phase angle between the stall signals at those three planes relative to the base plane. Then the first anemometer was moved to another plane and the second, again, was placed alternately in each of the remaining planes. This process was repeated until twelve phase angle measurements had been made as a result of using each of the four planes in turn as the base plane.

The edges of the stall cells are not as sharp as one would like for measurements of this type; that is, it is difficult to determine where the stall cell begins and ends. For this reason, the phase relationships were read for both the leading and trailing edges of the stalls, and the mean was calculated. Even with this averaging process, the scatter in the data was extremely wide. The mean phase angles of the disturbances recorded at each test plane relative to each base plane were plotted and superimposed to give the least scatter and the most consistent pattern. Examples of the superimposed data for full and partial span stalls in the three-stage free-vortex machine are shown in Figure 17. The scatter of these data indicates that the angle between the stall cell (extending through the machine) and the axis of the machine is very difficult to measure. This angle enters into some stall

propagation theories as an empirical parameter.

3.1.3 Full Stall Transition Zones. The flow in the transition zones of full stall was extremely turbulent and the time rate of change of velocity was apparently high. To determine at least an approximation to the flow conditions within the transition zones, the following analysis, based on a torque balance, was made.

The fraction, a , of the annulus supporting reversed flow during full stall propagation in the three-stage compressor was measured as a function of the flow rate and was found to behave as

$$a = 0.83 - 1.7\,\bar{\phi} \qquad \text{for} \qquad 0.1 \leq \bar{\phi} \leq 0.3 \quad .$$

The fraction, b , of the annulus involved in the transition zones was found to have a nearly constant value of 0.17 for the range of flow coefficients above.

Under the assumptions that the flow over the unstalled portion of the annulus was very near the design flow and remained so as a increased with decreasing $\bar{\phi}$, and that the reversed flow was locally constant at a mean measured value of $\phi_s = -0.08$, the torque caused by the flow through the unstalled and reversed portions of the annulus was calculated. The flow parameters used were measured at mid-radius and assumed to be near the true values averaged over the blade span.

The dimensionless torque on a full blade row is

$$\tau = \frac{\bar{r}\,\rho\, c_a\, A\, \Delta c_u}{\frac{1}{2}\rho\, u_o^2\, A\, r_o} \quad ,$$

or

$$\tau = 2\,\bar{\xi}\,\phi\,\lambda \quad ,$$

where

$$\bar{\xi} = \frac{\bar{r}}{r_o} \quad , \quad \phi = \frac{c_a}{u_o} \quad , \quad \lambda = \frac{\Delta c_u}{u_o} \quad .$$

The dimensionless torque caused by the flow through a fraction, f, of the annular area and flowing across three identical rotor rows is

$$\tau = 6 f \bar{\xi} \phi \lambda \quad .$$

Let

$$\tau = \tau_n + \tau_s + \tau_t \ ,$$

where

τ_n = torque caused by normal flow in unstalled area,

τ_s = torque caused by flow in reversed area,

τ_t = torque caused by flow in transition zones.

In terms of the parameters used to define the various areas of the flow,

$$\tau_n = 6(1 - a - b) \bar{\xi} \phi_n \quad n$$

$$\tau_s = 6 a \bar{\xi} \phi_s \quad s$$

$$\tau_t = 6 b \bar{\xi} \phi_t \quad t$$

Using the previously stated values of a and b, and $\phi_n = 0.41$, $\tau_n = 0.25$, $\phi_s = -0.08$, $\bar{\xi} = 0.8$, and $\lambda_s = -1.0$,

$$\tau = 0.32 + .18 \bar{\phi} + .82 \phi_t \lambda_t \quad .$$

It was impossible to evaluate ϕ_t and λ_t with precision even as limited as that of the other quantities in the calculation.

Over the limited range of $\bar{\phi}$ in question, the torque actually

measured on this same machine and reported in Reference 5 is related to $\bar{\phi}$ nearly linearly:

$$\tau \approx 0.53 - 0.30\,\bar{\phi} \quad .$$

If the torque calculated from the approximate measured flows is to be consistent with the torque measured on the dynamometer shaft, then

$$\tau_t = 0.21 - 0.48\,\bar{\phi} = 0.82\,\phi_t \lambda_t \quad .$$

If ϕ_t is constant and (judging from experimental results) a little higher than ϕ_n, say 0.50, then

$$\lambda_t \approx 0.50 - 1.2\,\bar{\phi} \quad ,$$

or

$$0.14 < \lambda_t < 0.38 \quad ,$$

as

$$0.30 > \bar{\phi} > 0.10 \quad .$$

This range of values for λ_t is not unreasonable, but the nature of the dependence of λ_t upon $\bar{\phi}$ is not understood.

3.2 Vector Velocities

3.2.1 Tangential Flow. The L-probe was used to measure the behavior of vector velocities in the flow fields of several blading configurations during stall propagation. The single cell partial span stall was chosen for most of this detailed study because of its relative simplicity and because it is frequently the first type of stall to appear in a machine as the flow rate is reduced from the point of maximum efficiency.

As a first approximation, radial flow was assumed to be negligible, since the radial component of velocity was difficult to measure and since it was believed (and later confirmed) that radial flow is significant only within and very near the stall cell itself.

The first configuration studied was an expanded free-vortex stage consisting of inlet guide vanes, the second rotor, and the third stator. The magnitudes (non-dimensionalized in terms of the rotor tip speed) of the total velocity, the whirl component, and the axial component as well as the flow angle, all measured immediately downstream of the rotor at five radial positions, are shown in Figure 18. The figure also shows a faithful reproduction of an oscilloscope photograph illustrating the selection of data points. Figure 19 depicts the radial distribution of velocity components at the point in the flow field midway between successive passages of the stall cell and compares these speeds to the same ones at a flow coefficient for which stalling was imminent, and with the design speeds. Also shown in Figure 19 is the radial distribution of angular velocity of the flow between passages of the stall cell.

Figure 20 is similar to Figure 19 but shows the radial distribution at survey planes 3, 5, and 7 of mean flow components between successive passages of the stall cell for a configuration consisting of free-vortex guide vanes and first rotor with no stator.

Figures 23 and 22 present data similar to that of Figures 18 and 19, but for stall propagating on a configuration consisting of solid body guide vanes and first rotor.

Figures 23 and 24 show data still similar to that for Figures 18 and 19, but for a single cell partial span stall propagating in the three-

stage free-vortex machine. These data were taken (prior to the design of the L-probe) with the V-probe, for which the accuracy during large angular excursions is considerably lower than that of the L-probe. For that reason, data were taken at a limited number of positions; two radial positions in front of and two behind the second stator.

The flow between successive passages of the full-span stall cell propagating on the three-stage free-vortex machine is shown in Figure 25. The radial distribution of the mean values of the whirl component of velocity and the angular velocity of the flow is given in Figure 26.

Table 2 summarizes propagation angular velocities of stalls described in Figures 18 - 26 as well as those of stalls on different blade configurations for which no detailed flow measurements were made. The table also includes measured average angular velocities of the flow between successive passages of the stall cells.

3.2.2 Radial Flow. The radial V-probe showed that throughout the partial span flow fields and in all areas of full stall but the transition zones (for which the flow was too turbulent to interpret the results), the radial component of flow was no larger than 20% of the total speed. This means that the assumption of two-dimensional flow for the measurements described above produced a maximum error of

$$1 - \cos\left(\sin^{-1}\frac{2}{10}\right) \approx 2\%\ .$$

For both partial and full-span stalls, radial flow was outward at the leading edges of the cells and inward at the trailing edges over the middle portion of the span. Partial stall exhibited notably less radial flow over the area between stall cells than did full stall. At

mid-radius, the reversed flow within the full stall cell immediately downstream from the rotors had an outward radial component of about 20% of the total speed, while immediately upstream an inward radial component of approximately the same magnitude was observed.

IV. DISCUSSION OF EXPERIMENTAL RESULTS

Table 2 suggests that stalls of the single-cell partial span type propagate at the angular velocity of the flow between successive passages of the stall cell averaged over the blade span immediately downstream from a relatively isolated blade row. Furthermore, stalls of the same type in a multistage machine composed of identical stages travel at the arithmetic mean of two such averages; one just upstream and one just downstream from any particular blade row.

Figure 18 shows that for a partial span stall traveling on a free-vortex rotor the whirl velocity just downstream of the rotor increases or decreases as necessary to match the local stall propagation velocity at all but one of the five radial positions investigated. This suggests that although large disturbance of the flow speed is confined to the tips of the rotor blades (thus making the stall "partial"), the disturbance actually extends over the whole span. It further suggests that the boundaries of the stall cell are formed by streamlines, since if the local velocity equals the stall velocity there is no flow into the stall cell.

Figure 21 shows similar results for a partial stall traveling on a solid-body rotor. In this case, however, the strong tendency for the whirl velocity to conform to the local stall velocity near the hub is absent.

Both Figures 18 and 21 show that for some portion of the span between the case and the point at which the mean whirl velocity of the flow between stall cells equals the local stall velocity, the whirl ve-

locity tends not to conform to the stall velocity as the stall passes.

As it is shown in Figure 15, the largest area of disturbance from the mean flow for a partial stall traveling in the three-stage machine is near the hub. Figure 23 shows that the whirl velocity is altered to conform to the local stall speed near the hub both upstream and downstream from the stator. At the test points near the case, the whirl velocity ahead of the stator between successive passages of the stall was nearly equal to the stall velocity, but behind the stator there was no tendency for the whirl velocity to conform to the stall. Thus, the concept of a stall cell the boundary of which is a streamtube is of limited utility.

Reference 16 was the first to observe experimentally that a stall cell propagating on an isolated rotor "propagates at the speed of the downstream whirl." The two-dimensional vortex-shedding theory of Reference 17 predicts the propagation velocity to be equal to the downstream whirl if the stall cell does not spiral around the machine axis downstream from the blade row. It is pointed out in References 1 and 19 that the angle of downstream spiral is very small in most reported cases. Reference 17 places the experimentally measured angle between the tangent to the stall cell and an element of a cylinder coaxial with the annulus at from -15° to $+19^{\circ}$. Figure 18 shows the difficulty of measuring this angle. Reference 17 also states that fair experimental agreement between the stall propagation velocity and the downstream whirl velocity has been noted by "other observers".

A properly designed compressor will stall fairly close to its design point, and, as has been shown here and suggested by several

investigators (e.g. see Reference 11), the flow conditions (at least in the mean) between stall cells remain about the same as the flow which occupied the whole annulus at the flow rate for which stalling was imminent. It is useful, then, to compare stall propagation angular velocities reported by other observers with the range of mid-radius angular velocities of the design flow for their respective machines, even though vector velocity measurements during stall were not made.

In Figure 27, absolute stall propagation angular velocity is plotted against design angular velocity at mid-radius for 18 reported cases of partial and full-span stalls. The design angular velocity is plotted as a bar, the right end of which represents the angular velocity downstream, and the left end of which represents the angular velocity upstream from the rotor. The line of equality between stall angular velocity and design flow angular velocity is drawn in.

The general trend of Figure 27 is for partial stalls on isolated rotors to be farthest from the line of equality to the left and for full stalls on complete single-stage machines to be farthest away to the right. Cases 2 and 4, which are referenced to this paper, are to the left of the line, although in Table 2 the angular velocity is reported to be very nearly equal to the angular velocity of the flow behind the rotor between successive passages of the stall cell. This is because the blades used were either isolated or separated from the stator blades they were designed to match and the downstream angular velocity of the flow was actually higher than the design value. The one case of full stall reported in Table 2 exhibits the general trend of Figure 27 that the angular velocity of full stall matches the flow behind the stators

much closer than it does an average over the rotors and stators.

Allowance for reasonable variation in the separation of design points and stall points among the different compressors reported and further allowance for the fact that the mean angular velocity of the flow does not occur at mid-radius for all machines shows that Figure 27 does not contradict the hypothesis that on isolated blade rows partial stalls travel at the mean downstream angular velocity of the flow between successive passages of the stall cells. The question which remains, however, is of the effect on the stall speed of flow through closely-spaced multiple blade rows.

Case 1 of Figure 27 shows a stall speed which seems to conform to the whirl flow just downstream from the rotor. Cases 7, 8 and 9 seem to conform to the average of flows on both the rotor and stator. Cases 11 and 13 seem to be governed exclusively by the stator. The conclusion must be that stall propagation speed is very sensitive to the particular design of a set of blades. The discussion below indicates that the very existence of a stable partial stall on a rotor is quite sensitive to the angle at which the stators are set, even in a single-stage machine.

With very few exceptions, compressor blades are designed for perfect fluid flow. Real fluid effects cause increased angles of attack on rotor blades near the case and on the stator blades near the hub.

Preliminary tests using a rectangular cascade in which the flow near one wall was twisted by a row of vanes upstream to simulate the conditions of a moving wall revealed that 25% of the area of the suction side of the blades was in separated flow at the angle of attack for max-

imum lift-to-drag ratio as given in Reference 25. The area of separated flow was roughly triangular in shape, and covered 85% of the chord at the wall on which the flow was twisted and about 30% of the span along the trailing edge. Although a propagating disturbance was found on the cascade, its properties were difficult to study because of the wakes shed by the upstream turning vanes.

Stalls involving only a portion of the blade span would seem to be a natural result of the fact that near a relatively moving wall the blades are subjected to angles of attack higher than those for which they were designed. Most compressors exhibit partial stalls near the case, i.e. on the rotors. The three-stage free-vortex machine described in this paper is one of the few machines to evidence partial stall near the hub, i.e. on the stators.

In the free-vortex machine consisting of guide vanes, second rotor, and third stator, a fairly stable flow could be attained with stall propagating on the stators when the stator blades were turned so as to increase their angles of attack. The stall was clearly on the stators, for while it resembled any other stall behind the stator, it was detectable only as a small amplitude potential-type disturbance immediately behind the rotor.

It might be expected that compressors would stall on either the case or the hub depending upon whether the real angles of attack were farther from design on the tips of the rotors or stators, respectively. Experiments with different stator angles on the various machine configurations used to compile Table 2 were conducted. In most cases, irregular disturbed flow was detected near the hub at flow rates higher

than those for which clearly-defined case stalls were established on the rotor. As the flow rate was decreased, the flow near the hub would gradually become as regular as that near the case and then, suddenly, a stall would begin to propagate on the rotor. Multiple-cell rotor stalls could be established at virtually any stator angle, but in some cases the existence of the pre-stall irregular flow near the hub was prerequisite to the establishment of a stable single-cell rotor stall.

Figure 25 shows that the angle of attack on both rotor and stator blades decreases (rather than increases) as the full stall cell approaches. Full stall, then, is a phenomenon quite different in character from the simple concepts of Figure 1.

REFERENCES

1. Members of the Compressor and Turbine Research Division, "Aerodynamic Design of Axial Flow Compressors," vol. III, Lewis Flight Propulsion Laboratory, NACA RM E56B03b (1956).

2. Chesire, L. J., "The Design and Development of Centrifugal Compressors for Aircraft Gas Turbines," Proceedings of the Institute of Mechanical Engineers (1945), vol. 153, pp. 426-440.

3. Emmons, H. W., Pearson, C. E., and Grant, H. P., "Compressor Surge and Stall Propagation," Transactions of the American Society of Mechanical Engineers (1953), vol. 77, pp. 453-467.

4. Huppert, M. C., and Benser, W. A., "Some Stall and Surge Phenomena in Axial-Flow Compressors," Journal of the Aeronautical Sciences (1953), vol. 20, pp. 833-845.

5. Iura, T., and Rannie, W. D., "Observations of Propagating Stall in Axial Flow Compressors," California Institute of Technology, Report No. 4, Navy Contract N6-ORI-102, Task Order IV, (1953).

6. Sears, W. R., "A Theory of 'Rotating Stall' in Axial-Flow Compressors," Cornell University, Contract AF 33(038)-21406, U. S. Air Force Office of Scientific Research, (1953).

7. Marble, F. E., "Propatation of Stall in a Compressor Blade Row," California Institute of Technology, Technical Report No. 4, Contract AF 18(600)-178, U. S. Air Force Office of Scientific Research, (1954).

8. Stenning, A. H., "Stall Propagation in a Cascade of Airfoils," Massachusetts Institute of Technology, Report No. 5, NACA Contract NAw-6303, (1954).

9. Benenson, D. M., "Characteristics of Propagating Stall in Axial Flow Compressors," Ph. D. Thesis, California Institute of Technology, (1957).

10. Meyer, R. F., "An Experimental Study of Rotating Stall in a Two-Stage Axial Compressor," Aeronautical Report LR-259, National Research Council of Canada, (1959).

11. Siestrunck, R., Fabri, J., and Jarlan, L., "Étude des Régimes Critiques non Stationnaires dans le Fonctionnement a Vitesse Réducite des Compresseurs d'Aviation," Comptes Rendus des Journées Internationales de Sciences Aéronautiques, Office National d'Études et de Recherches Aéronautiques, (1957).

12. Bowen, J. T., Sabersky, R. H., and Rannie, W. D., "Theoretical and Experimental Investigation of Axial Flow Compressors," California Institute of Technology, Navy Contract N6-ORI-102, Task Order IV, (1949).

13. Alsworth, C. C., and Iura, T., "Theoretical and Experimental Investigations of Axial Flow Compressors, Part 3, Progress Report on Loss Measurements in Vortex Blading," California Institute of Technology, Navy Contract N6-ORI-102, Task Order IV, (1951).

14. Willis, J. B., "Review of Hot Wire Anemometry," Report ACA-19, Australian Council for Aeronautics, (1945).

15. Lowell, H. H., "Design and Applications of Hot-Wire Anemometers for Steady-State Measurements at Transonic and Supersonic Air Speeds," Lewis Flight Propulsion Laboratory, NACA TN 2117, (1950).

16. Schulze, W. M., Erwin, J. R., and Westphal, W. R., "Investigation of an Impulse Axial-Flow Compressor Rotor over a Range of Blade Angles," Langley Aeronautical Laboratory, NACA RM L50F27a, (1950).

17. Kriebel, A. R., Seidel, B. S., and Schwind, R. G., "Stall Propagation in a Cascade of Airfoils," Massachusetts Institute of Technology, NACA TN 4134, (1958).

18. Moore, F. K., "Research on Rotating Stall in Axial Flow Compressors, Part IV, A Preliminary Study of Three-Dimensional Rotating Stall," Cornell Aeronautical Laboratory, Inc., WADC Technical Report 59-75, (1959).

19. Delio, G. J., and Stiglic, P. M., "Experimental Investigation of Control Signals and the Nature of Stall and Surge Behavior in a Turbojet Engine," Lewis Flight Propulsion Laboratory, NACA RM E54I15, (1954).

20. Huppert, M. C., "Preliminary Investigation of Flow Fluctuations During Surge and Blade Row Stall in Axial-Flow Compressors," Lewis Flight Propulsion Laboratory, NACA RM E52E28, (1952).

21. Costilow, E. L., and Huppert, M. C., "Rotating-Stall Characteristics of a Rotor with High Hub-Tip Radius Ratio," Lewis Flight Propulsion Laboratory, NACA TN 3518, (1955).

22. Costilow, E. L., and Huppert, M. C., "Some Effects of Guide-Vane Turning and Stators on the Rotating Stall Characteristics of a High Hub-Tip Ratio Single Stage Compressor," Lewis Flight Propulsion Laboratory, NACA TN 3711, (1956).

23. Turner, R. C., Hargest, T. J., and Burrows, R. A., "Stall Cell Propagation in Two Mismatched Compressor Stages," Aeronautical Research Council, C. P. No. 449, (1959).

24. Graham, R. W., and Vasily, D. P., "Experimental and Theoretical Investigations of Rotating-Stall Characteristics of Single-Stage Axial Flow Compressor with Hub-Tip Ratio of 0.76," Lewis Flight Propulsion Laboratory, NACA RM E53I09, (1953).

25. Emery, J. C., Herrig, L. J., Erwin, J. R., and Felix, A. R., "Systematic Two-Dimensional Cascade Tests of NACA 65 Series Compressor Blades at Low Speeds," NACA Report 1368, (1958).

FREE VORTEX $\left[C_{u1} = .145 \frac{r_0}{r} u_0 ;\ C_{u2} = .345 \frac{r_0}{r} u_0\right]$

	ROTOR					STATOR				
SECTION LOCATION - r - INCHES	10.8	12.6	14.4	16.2	18.0	10.8	12.6	14.4	16.2	18.0
DESIGN ENT. ANGLE - ROTOR - β_1 - DEG.	51° 21′	42° 24′	36° 2′	31° 21′	27° 45′					
DESIGN ENT. ANGLE - STATOR - γ_2 - DEG.						38° 3′	42° 24′	46° 13′	49° 34′	52° 31′
DESIGN EXIT ANGLE - ROTOR - β_2 - DEG.	86° 49′	65° 17′	50° 40′	41° 3′	34° 29′					
DESIGN EXIT ANGLE - STATOR - γ_1 - DEG.						61° 46′	65° 17′	68° 4′	70° 18′	72° 8′
SECTION CAMBER - θ - DEGREES	46° 40′	31° 0′	20° 19′	13° 47′	9° 48′	31° 53′	31° 6′	29° 59′	28° 41′	27° 20′
CASCADE STAGGER ANGLE - β' - DEG.	74° 48′	57° 54′	46° 12′	38° 15′	32° 36′					
CASCADE STAGGER ANGLE - γ - DEG.						54° 0′	57° 57′	61° 12′	63° 55′	66° 11′
SOLIDITY - C/S	1.150	.985	.862	.766	.690	1.035	.970	.920	.880	.849
MAXIMUM THICKNESS - % C	12	11	10	9	8	10	10	10	10	10

SOLID BODY $\left[C_{u1} = .325 \frac{r}{r_0} u_0 ;\ C_{u2} = \left(.325 \frac{r}{r_0} + .200 \frac{r_0}{r}\right) u_0\right]$

	ROTOR					STATOR				
SECTION LOCATION - r - INCHES	10.8	12.6	14.4	16.2	18.0	10.8	12.6	14.4	16.2	18.0
DESIGN ENT. ANGLE - ROTOR - β_1 - DEG.	52° 10′	46° 18′	40° 30′	34° 42′	28° 43′					
DESIGN ENT. ANGLE - STATOR - γ_2 - DEG.						48° 22′	46° 15′	42° 40′	37° 21′	29° 18′
DESIGN EXIT ANGLE - ROTOR - β_2 - DEG.	83° 7′	70° 47′	58° 19′	45° 33′	31° 48′					
DESIGN EXIT ANGLE - STATOR - γ_1 - DEG.						69° 30′	65° 18′	60° 36′	55° 11′	48° 41′
SECTION CAMBER - θ - DEGREES	40° 52′	32° 45′	24° 6′	14° 49′	4° 15′	28° 23′	25° 53′	24° 37′	24° 42′	27° 0′
CASCADE STAGGER ANGLE - β' - DEG.	72° 36′	62° 41′	52° 33′	42° 7′	30° 51′					
CASCADE STAGGER ANGLE - γ - DEG.						62° 34′	59° 12′	54° 59′	49° 42′	42° 48′
SOLIDITY - C/S	1.150	1.061	.995	.944	.903	1.039	.970	.920	.880	.850
MAXIMUM THICKNESS - % C	12	11	10	9	8	10	10	10	10	10

TABLE 1 BLADE DESIGN, FREE VORTEX AND SOLID BODY

TYPE BLADING	CONFIGURATION	TYPE STALL	SURVEY PLANE OF $\bar{\omega}/\omega_o$	$\bar{\omega}/\omega_o$	ω_s/ω_o
SOLID BODY	$V_1R_1 - - - - - V_2V_3$	PARTIAL	3	.69	.71
FREE VORTEX	$V_1R_1S_1R_2S_2R_3S_3\ V_2V_3$	FULL	6	.26	.26
↓	$V_1R_1S_1R_2S_2R_3S_3\ V_2V_3$	PARTIAL	(AV. 5 & 6)	.38	.38
	$V_1 - - R_2 - - S_3\ V_2V_3$	↓	5	.62	.63
	$V_1R_1 - - - - - V_2V_3$		3	.60	.61
	$V_1R_1 - - - - S_3\ V_2V_3$				.61
	$V_1R_1 - - S_2 - - V_2V_3$		NOT MEASURED		.61
	$V_1R_1S_1 - - - - V_2V_3$				.49
	$V_1 - - R_2S_2 - - V_2V_3$				.55

TABLE 2: SUMMARY OF MEASURED AVERAGE ANGULAR VELOCITIES OF FLOW BETWEEN STALL CELLS ($\bar{\omega}/\omega_o$) AND STALL ANGULAR VELOCITIES (ω_s/ω_o)

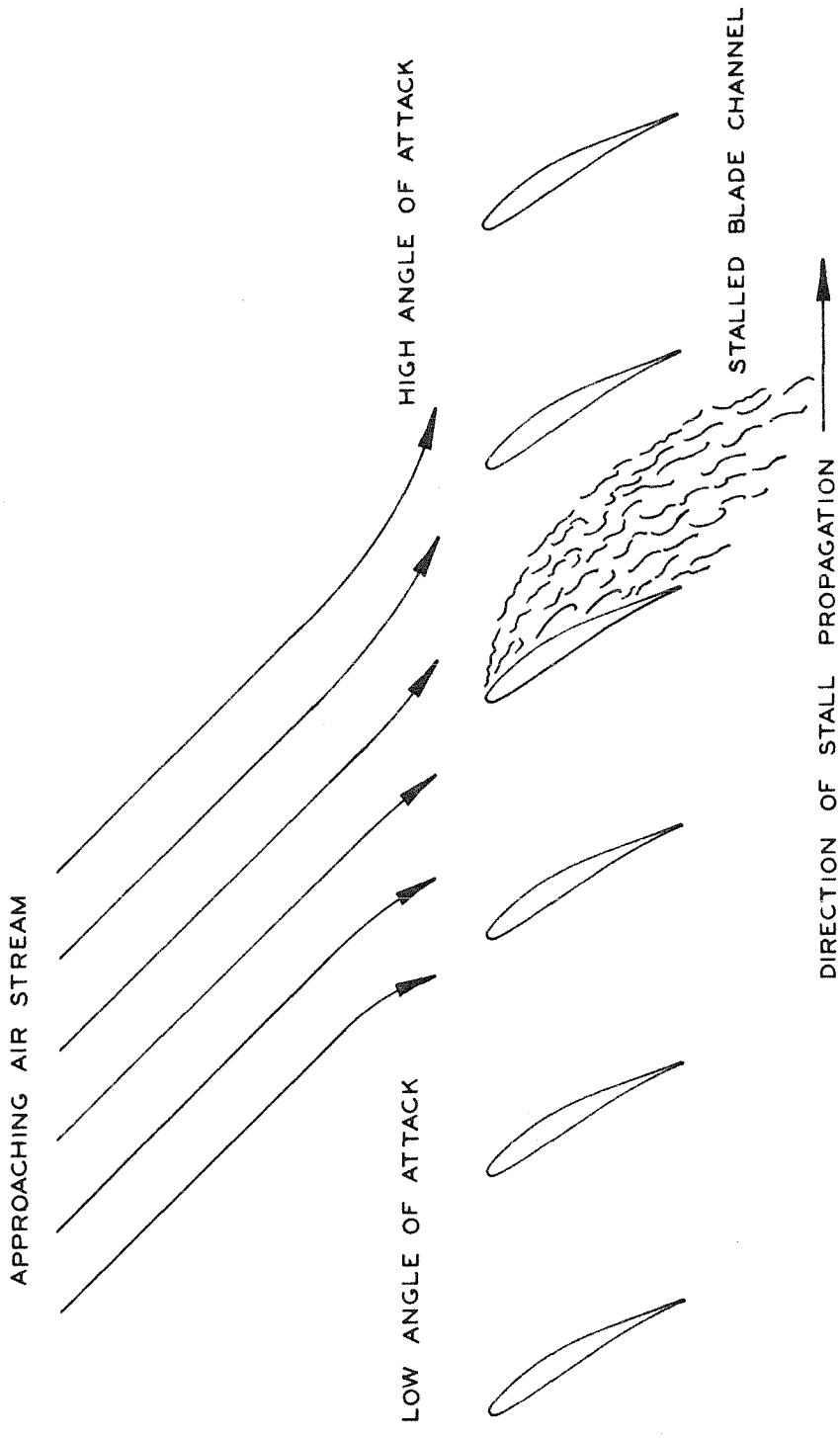

FIG. 1 STALL PROPAGATION IN A CASCADE

PRINCIPAL DIMENSIONS

NOMINAL TIP DIAMETER	36.000 INCHES
HUB DIAMETER	21.600 INCHES
HUB RATIO	.60
BLADE LENGTH	7.20 INCHES
BLADE CHORD	2.00 - 3.40 INCHES
NUMBER OF ROTOR BLADES	30 PER ROW
NUMBER OF STATOR BLADES	32 PER ROW
STAGES	1 TO 3
SPEED RANGE	0 TO 1800 R.P.M.
TIP SPEED RANGE	0 TO 283 FT./SEC.
AXIAL SPACING BETWEEN ROTOR & STATOR ℄	2.875 INCHES
AVERAGE AXIAL CLEARANCE BETWEEN ROTOR & STATOR	80 INCHES

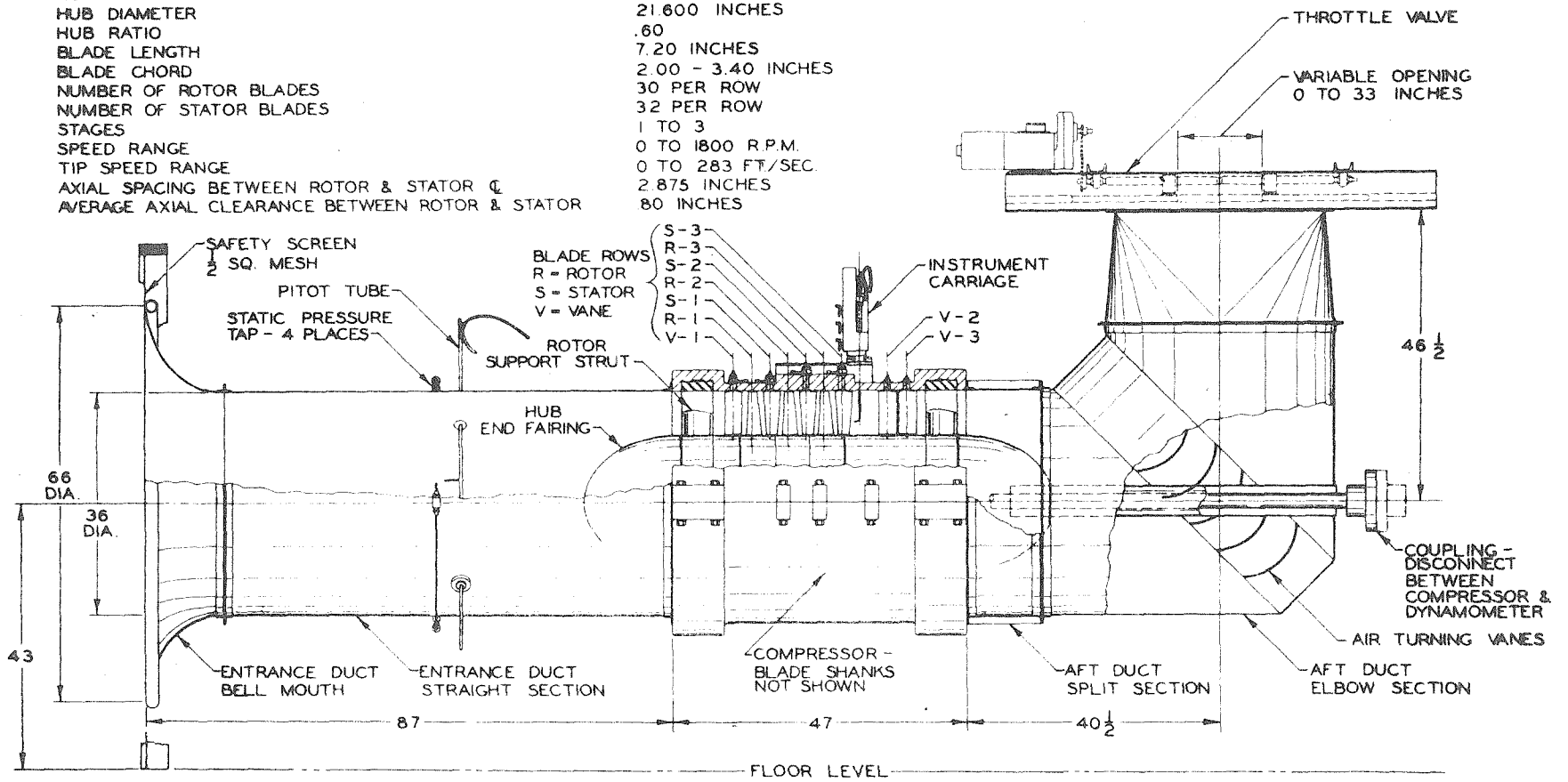

Fig. 2 Assembly Drawing of the Test Installation

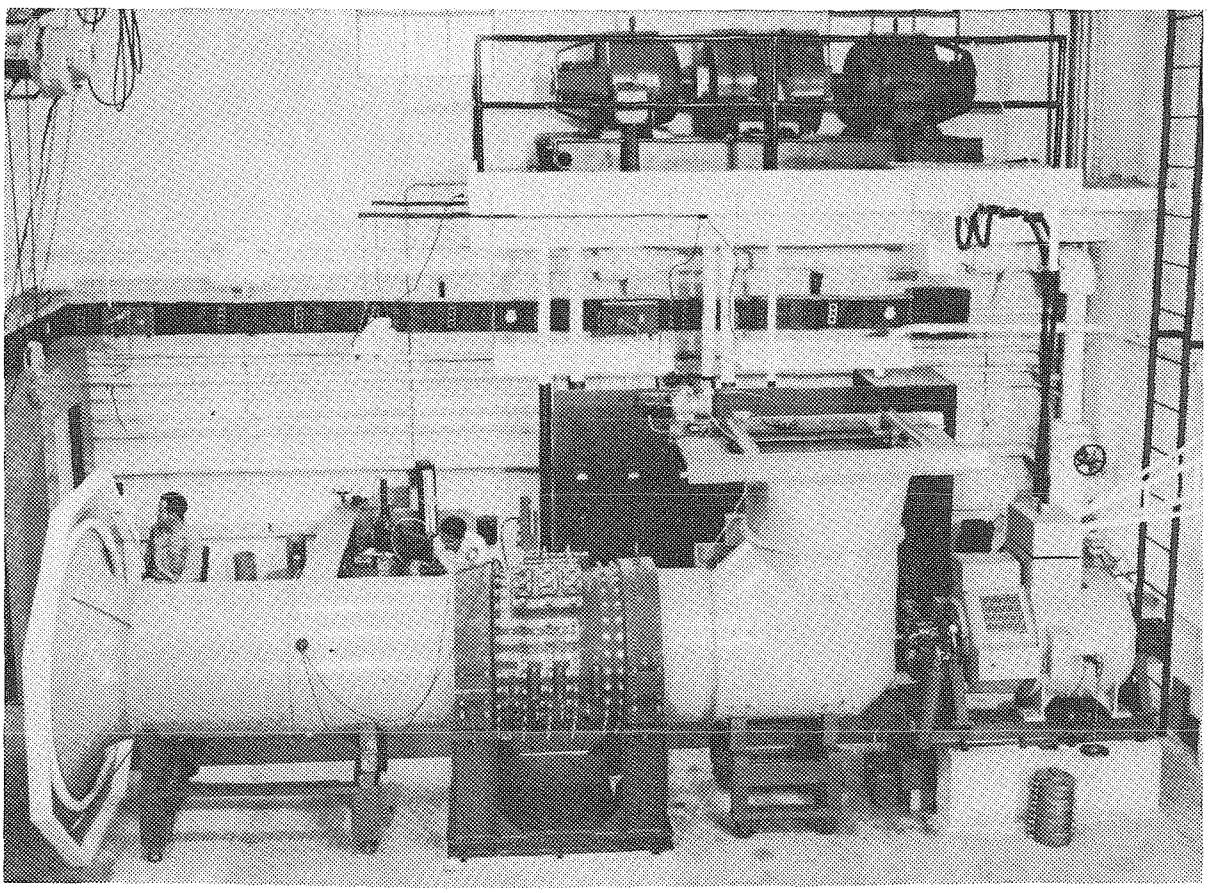

FIG. 3 AXIAL-FLOW COMPRESSOR

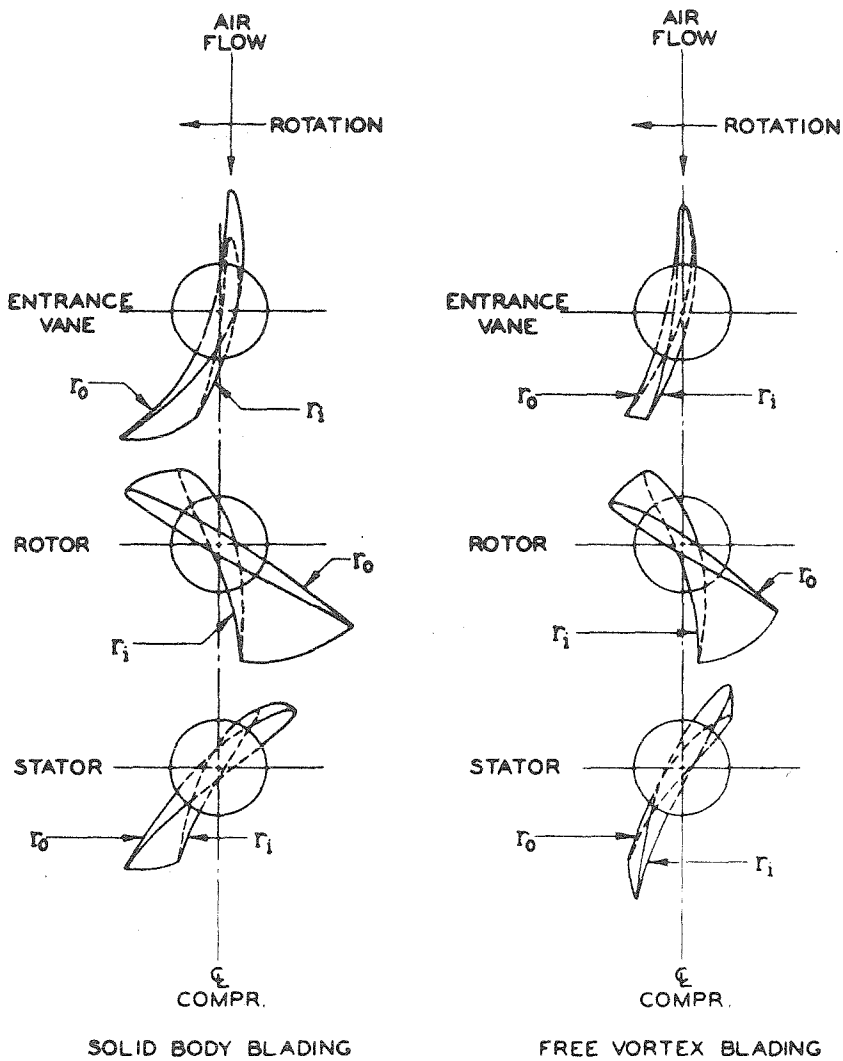

Fig. 4: Root and Tip Sections of the Two Types of Compressor Blading

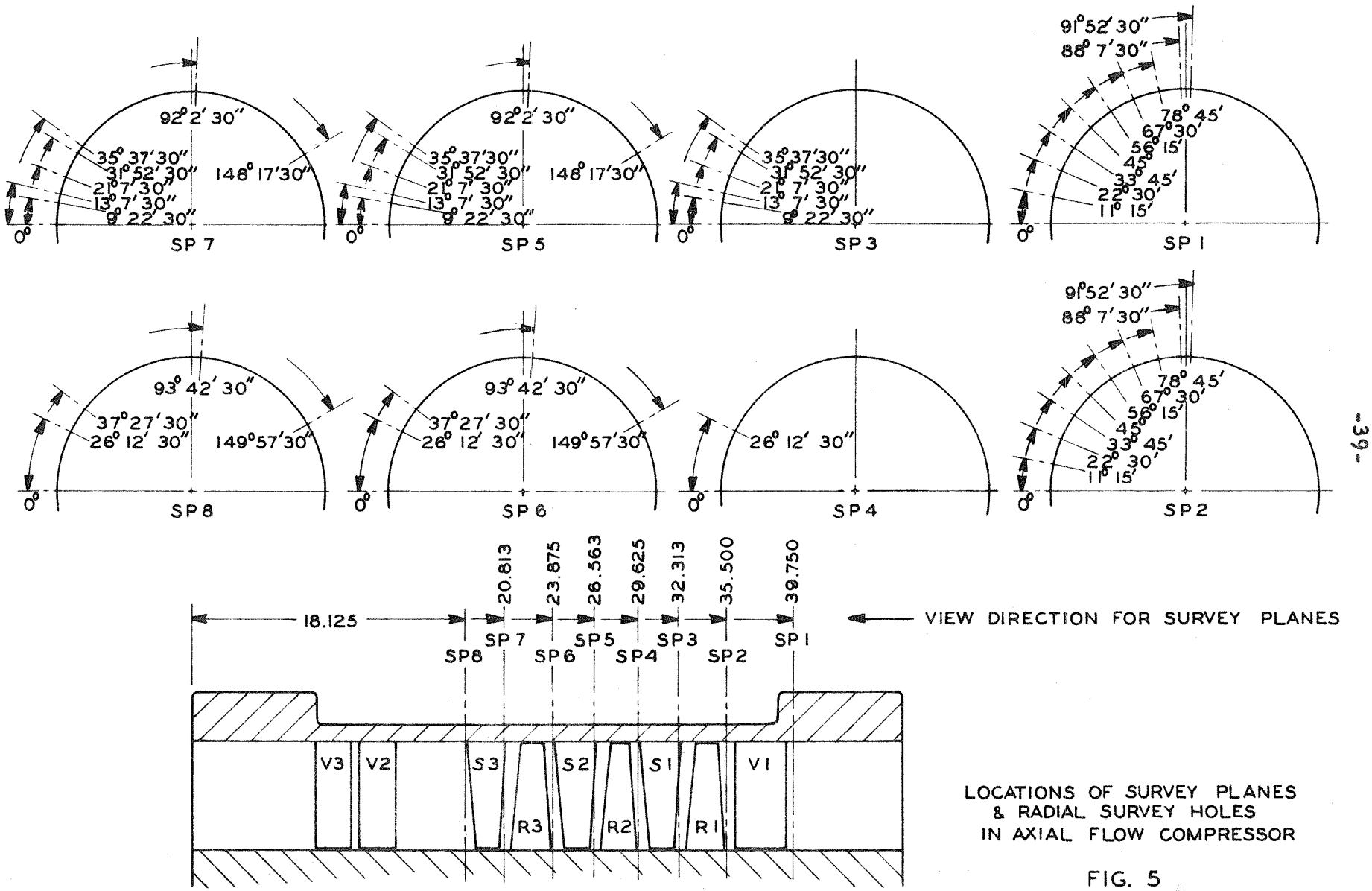

LOCATIONS OF SURVEY PLANES
& RADIAL SURVEY HOLES
IN AXIAL FLOW COMPRESSOR

FIG. 5

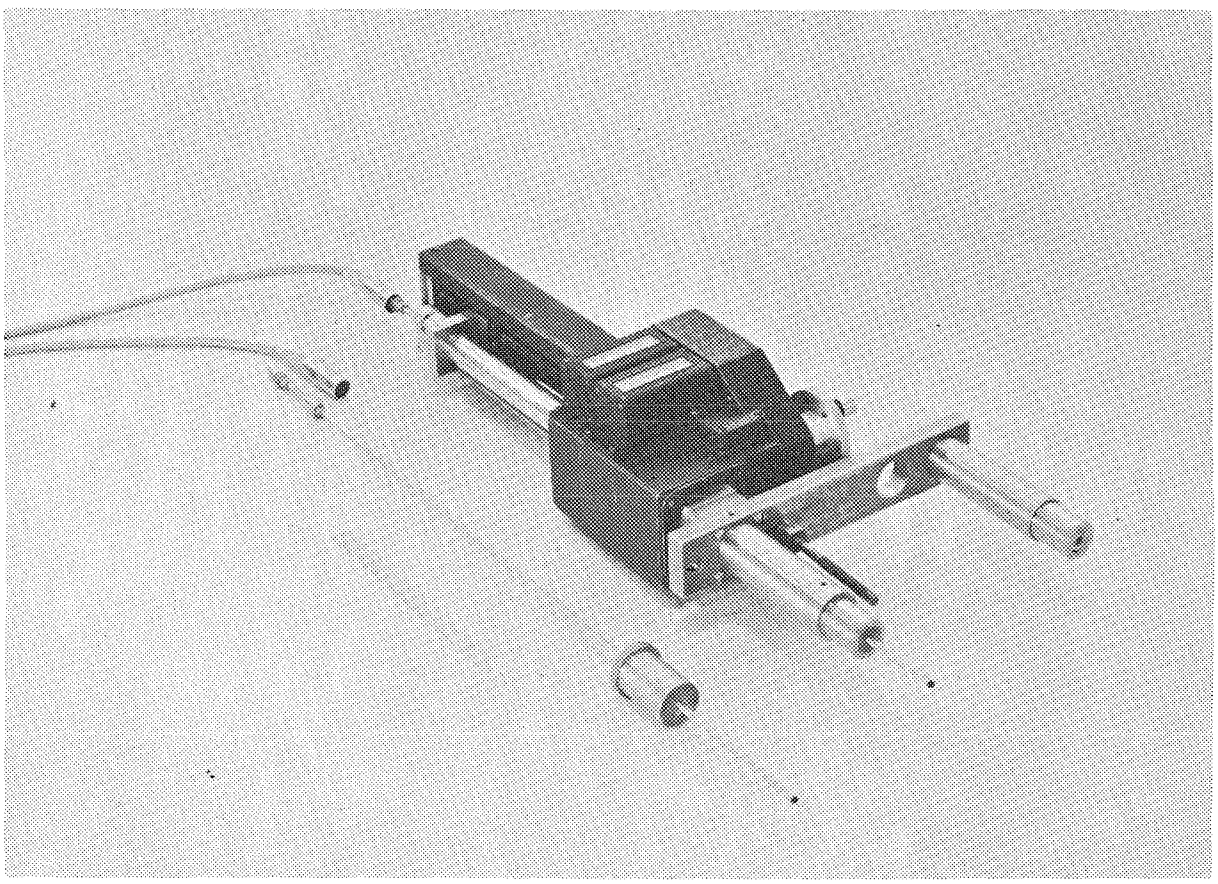

FIG. 6 RADIAL SURVEY CARRIAGE

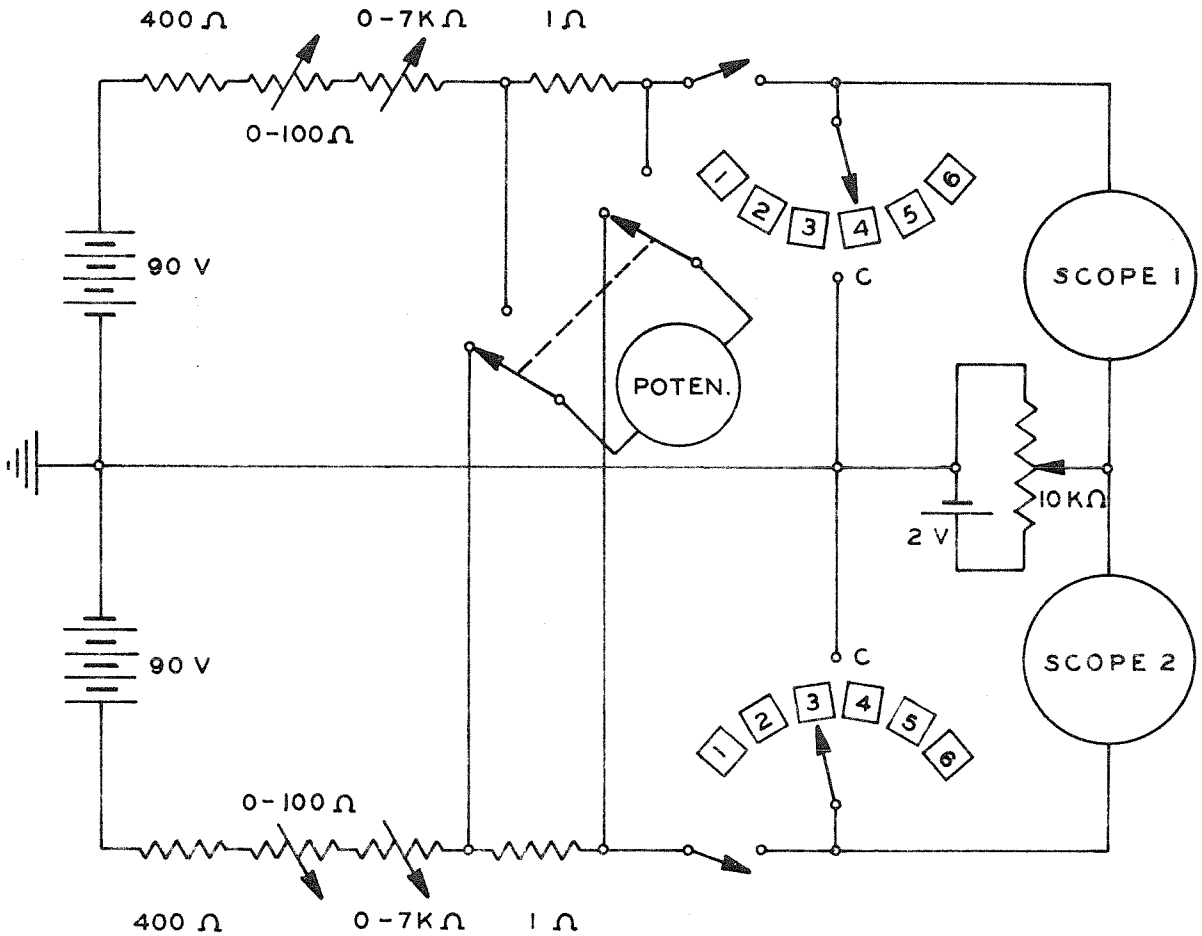

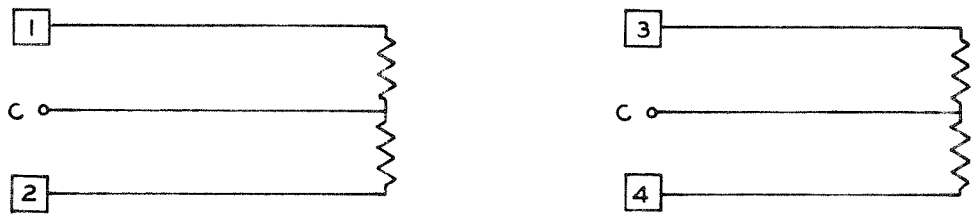

2 WIRE ANAMOMETERS

1 WIRE ANAMOMETERS

FIG. 7 HOT WIRE CIRCUIT

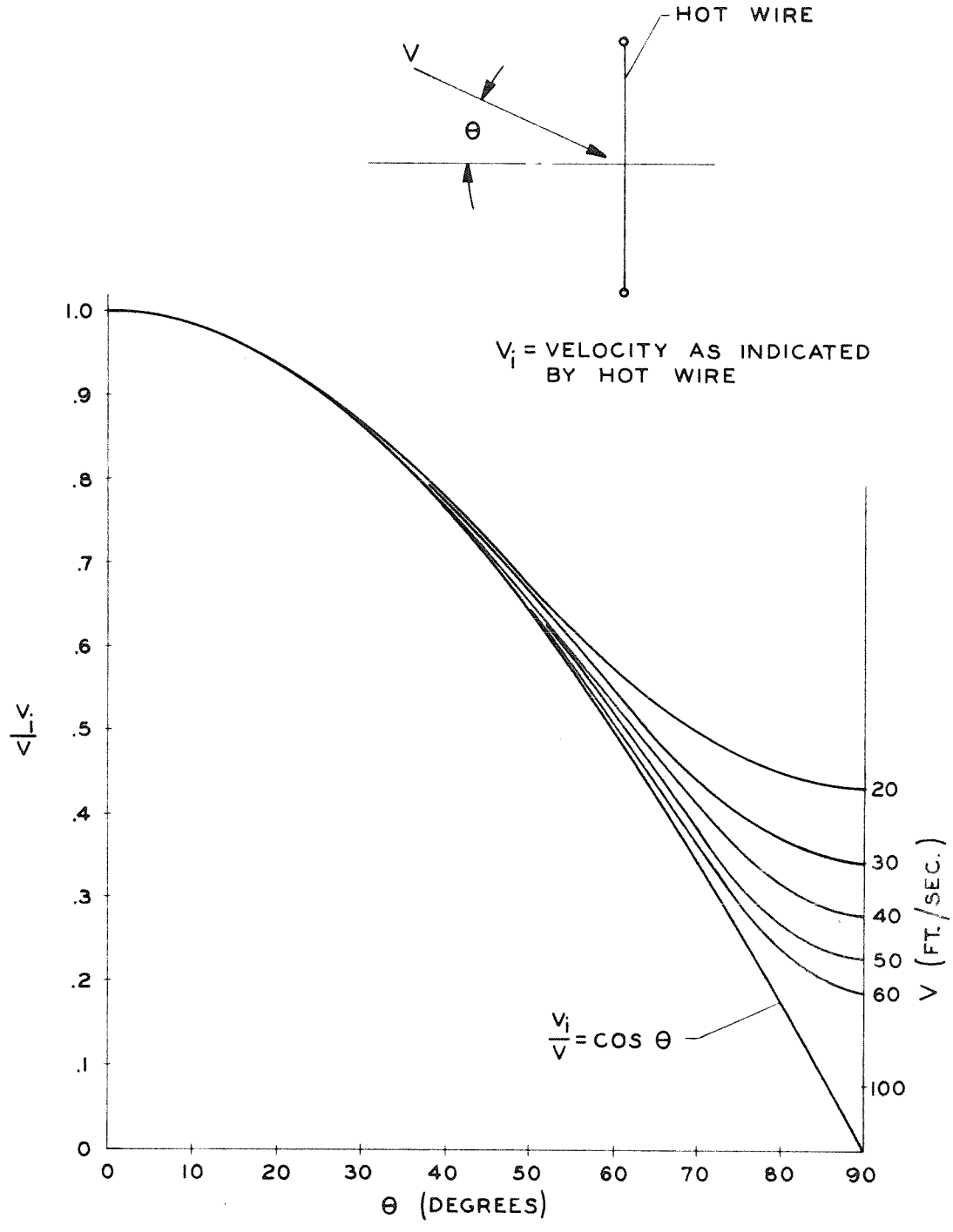

FIG. 8 ANGULAR BEHAVIOR OF HOT WIRES

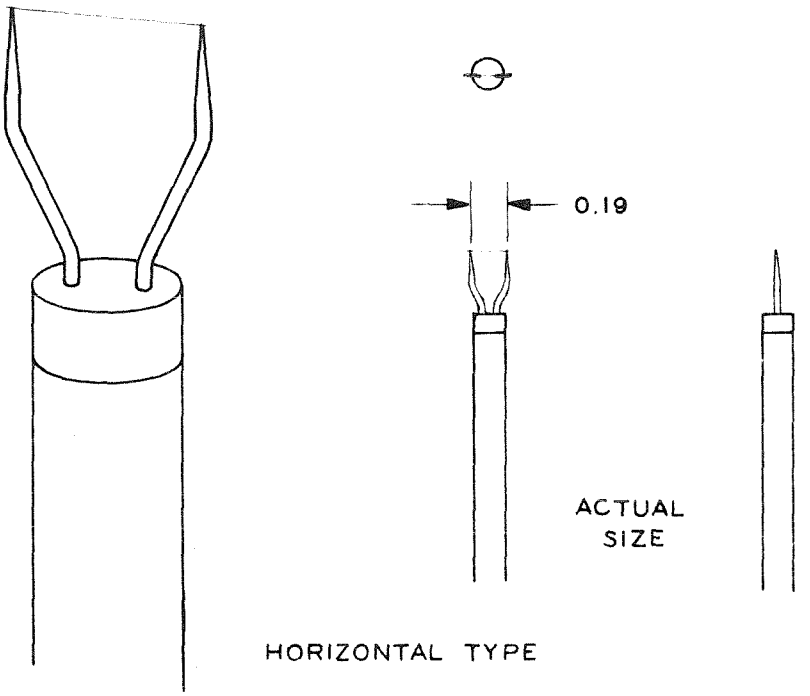

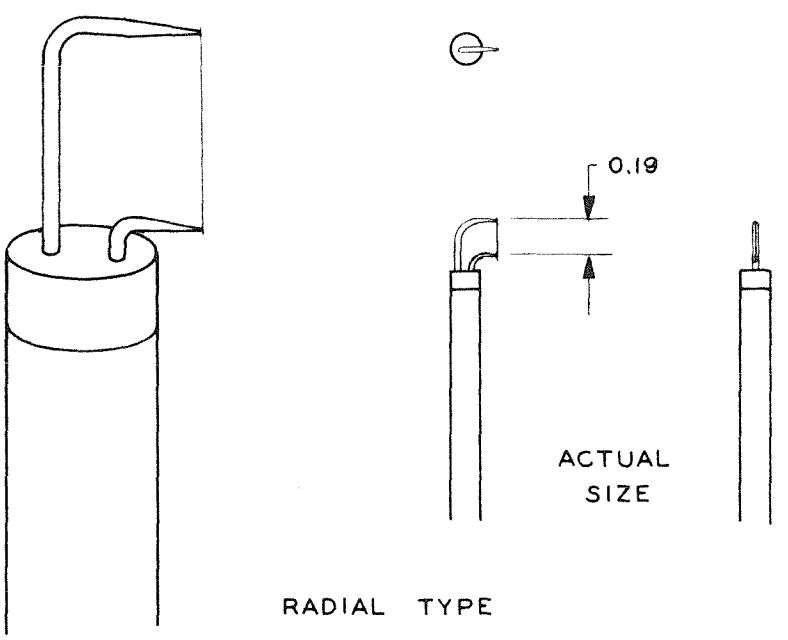

FIG. 9 SINGLE WIRE ANEMOMETERS

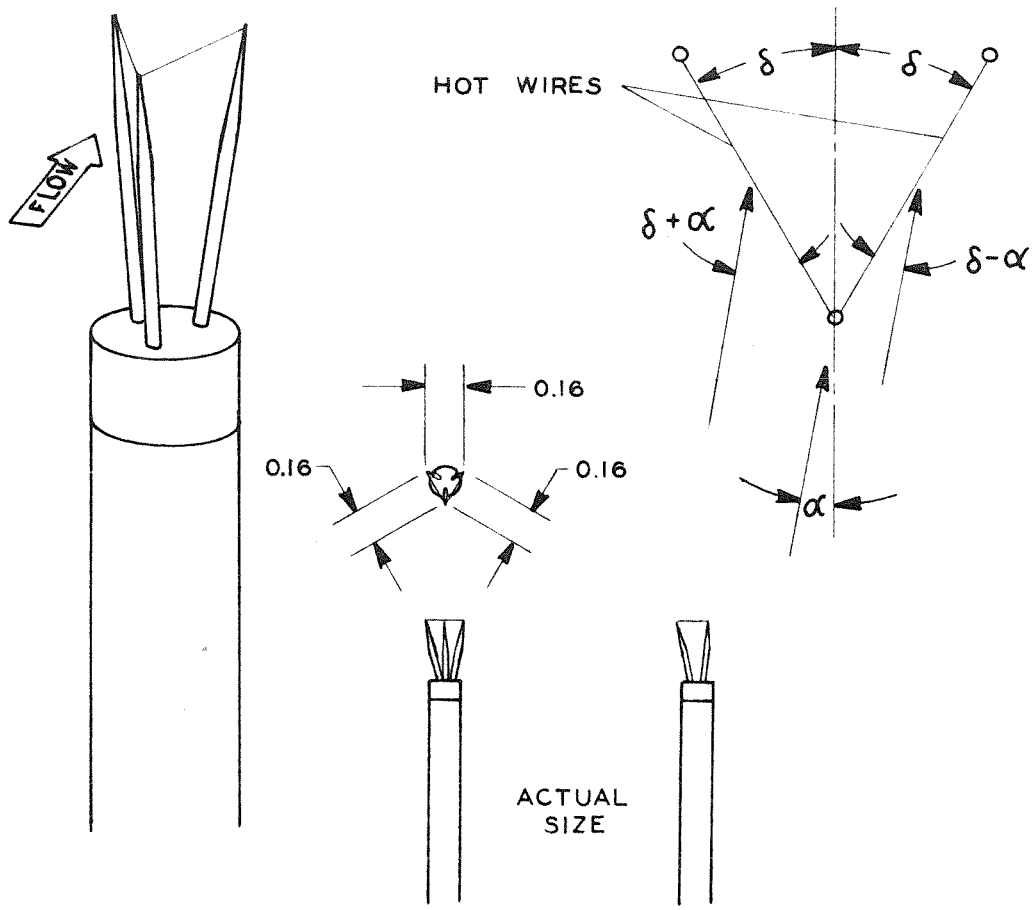

FIG. 10 "V" TYPE, DIRECTIONAL ANEMOMETER

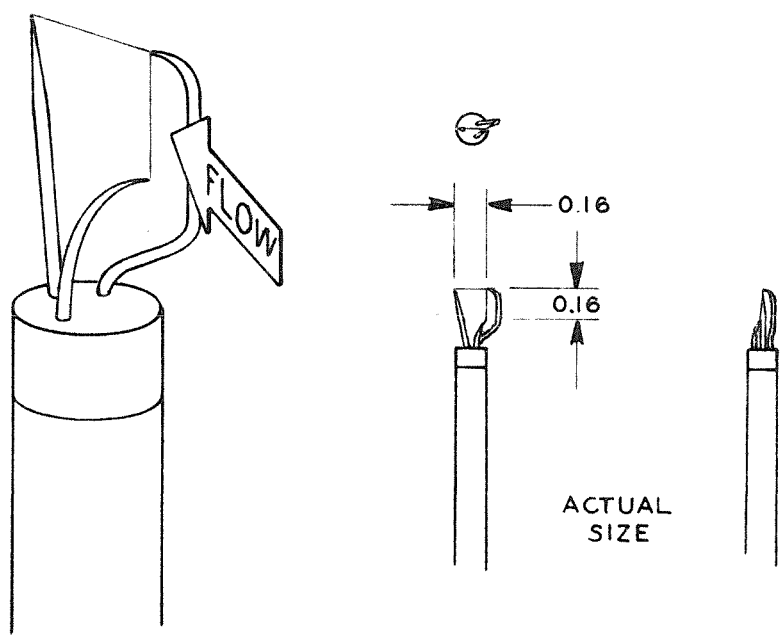

FIG. 11 "L" TYPE, DIRECTIONAL ANEMOMETER

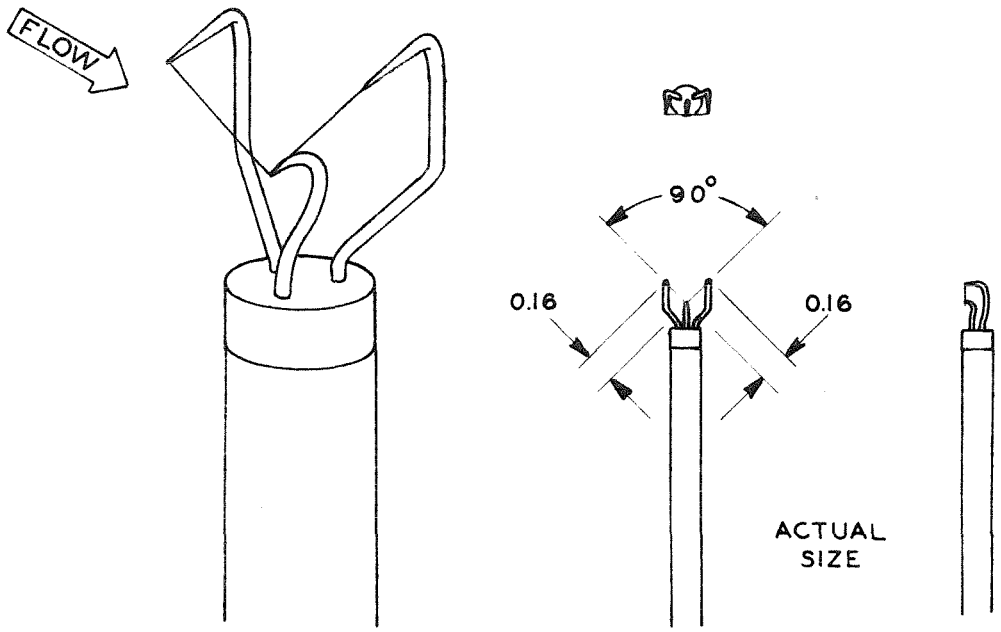

FIG. 12 RADIAL "V" ANEMOMETER

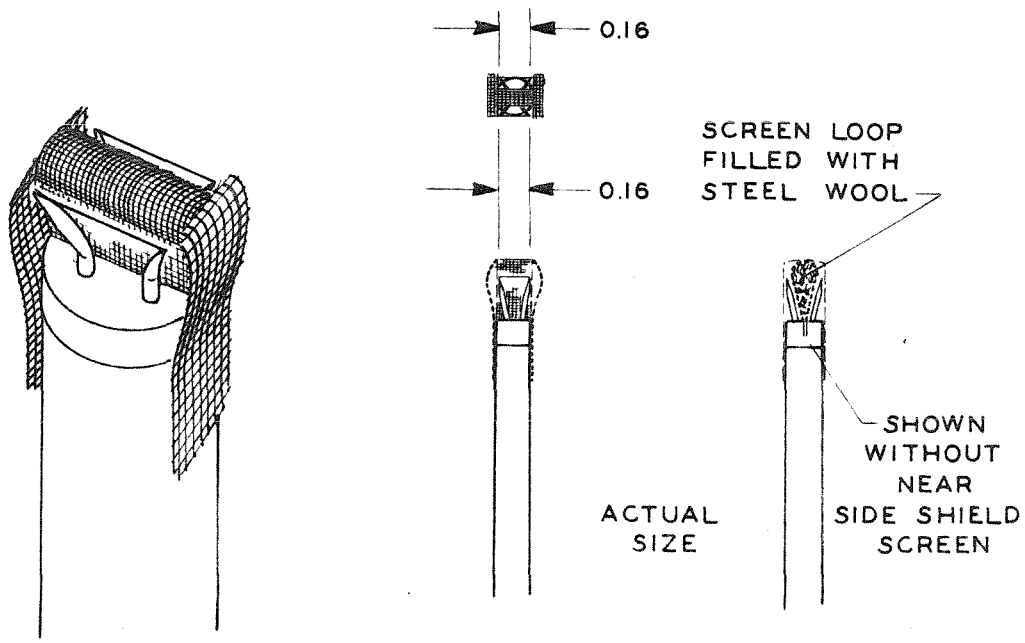

FIG. 13 FLOW REVERSAL ANEMOMETER

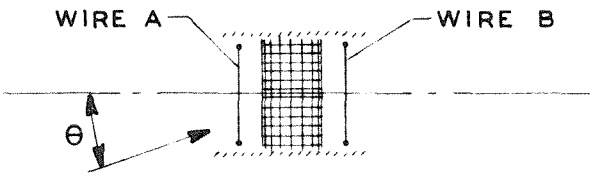

PROBE DIAGRAM

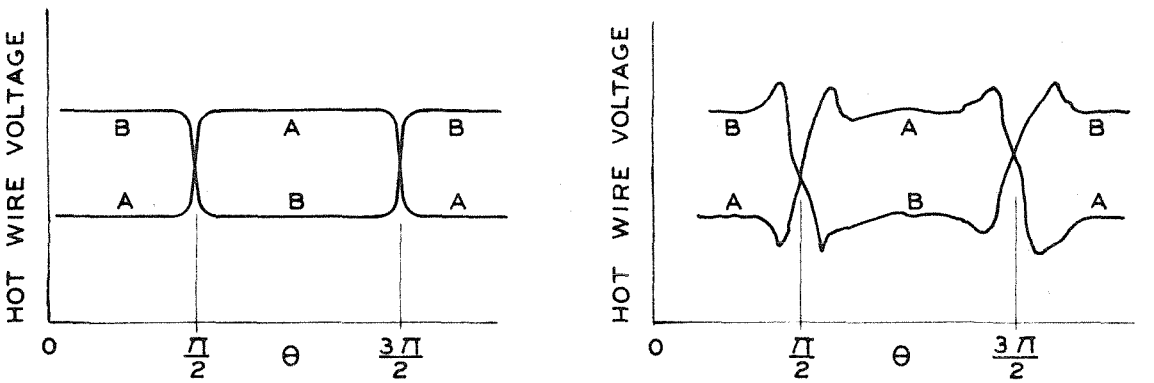

(A) DESIRED (B) OBTAINED

ANGULAR BEHAVIOR FOR CONSTANT INCIDENT SPEED

PROBE/FLOW DIAGRAMS. (LGTH. OF ARROW INDICATES RELATIVE VELOCITY)

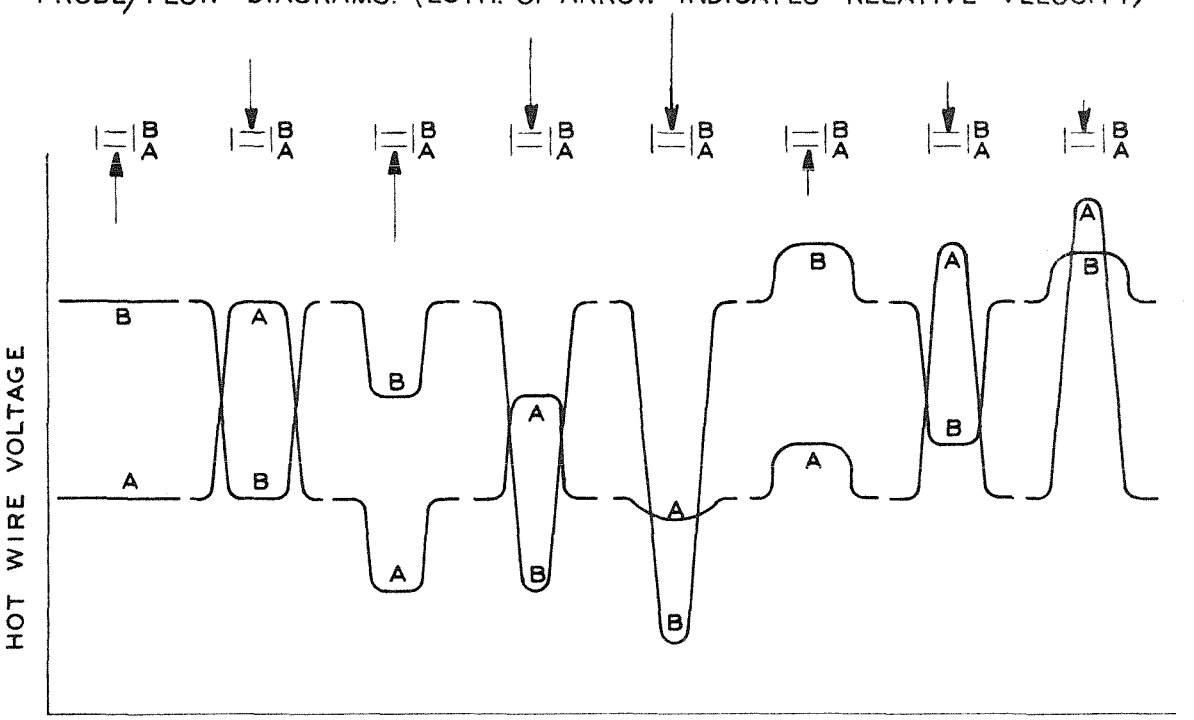

(C) RESPONSE UNDER VARIOUS FLOW CONDITIONS

FIG. 14 CHARACTERISTICS OF FLOW REVERSAL PROBE

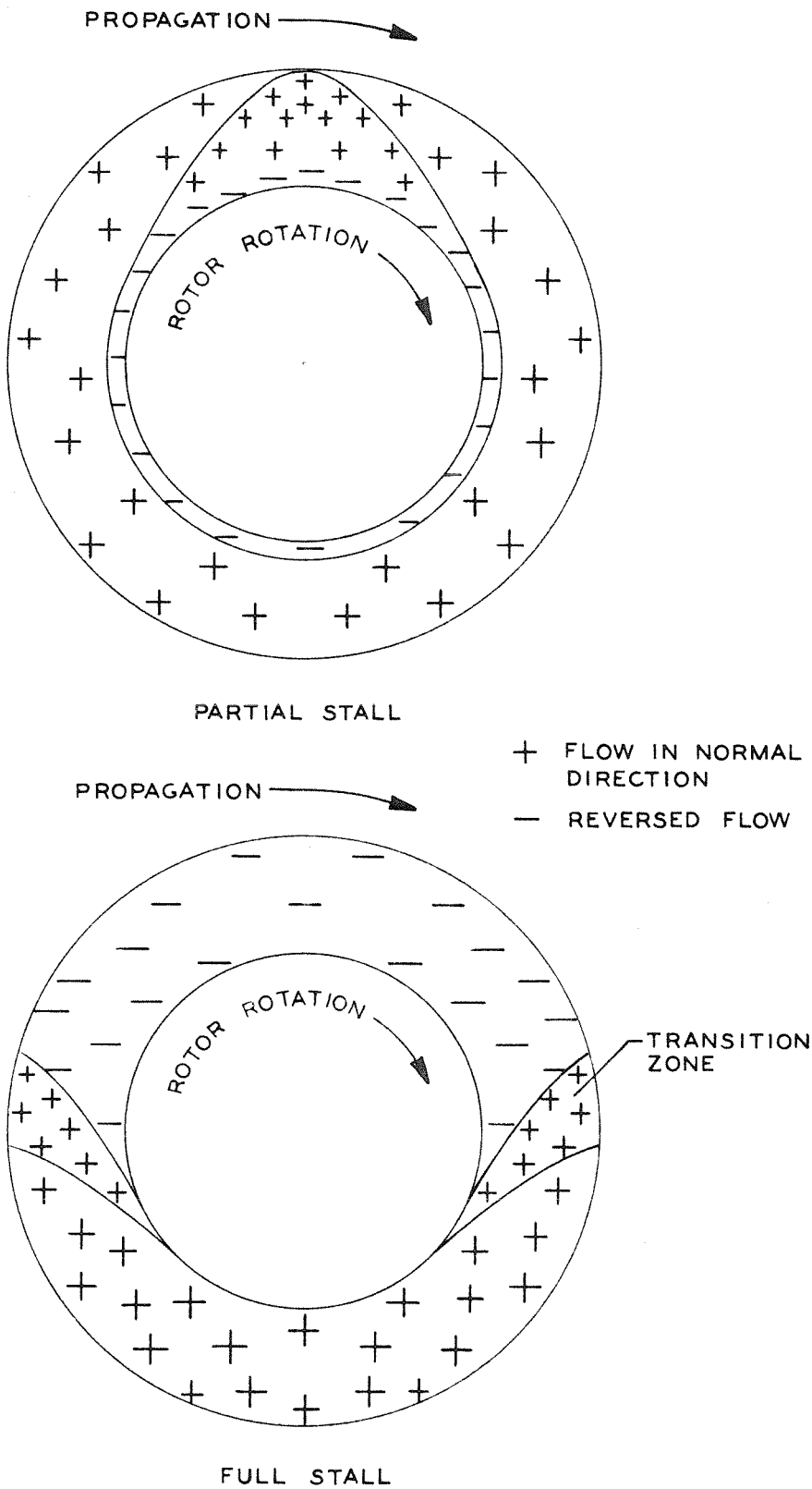

FIG. 15 AXIAL FLOW CHARACTERISTICS

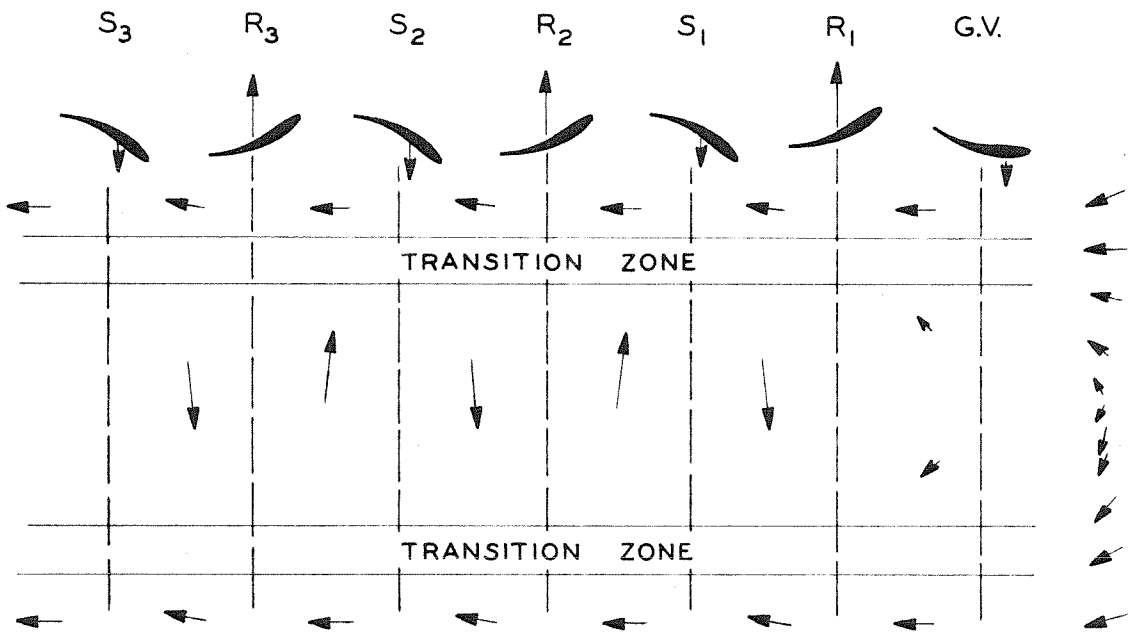

VELOCITIES ARE RELATIVE TO STALL CELL AT MID-RADIUS

ABSOLUTE ROTOR VELOCITY = ⟶

FIG. 16 QUALITATIVE DISTRIBUTION OF FLOW FOR FULL STALL ON THREE-STAGE, FREE-VORTEX BLADES

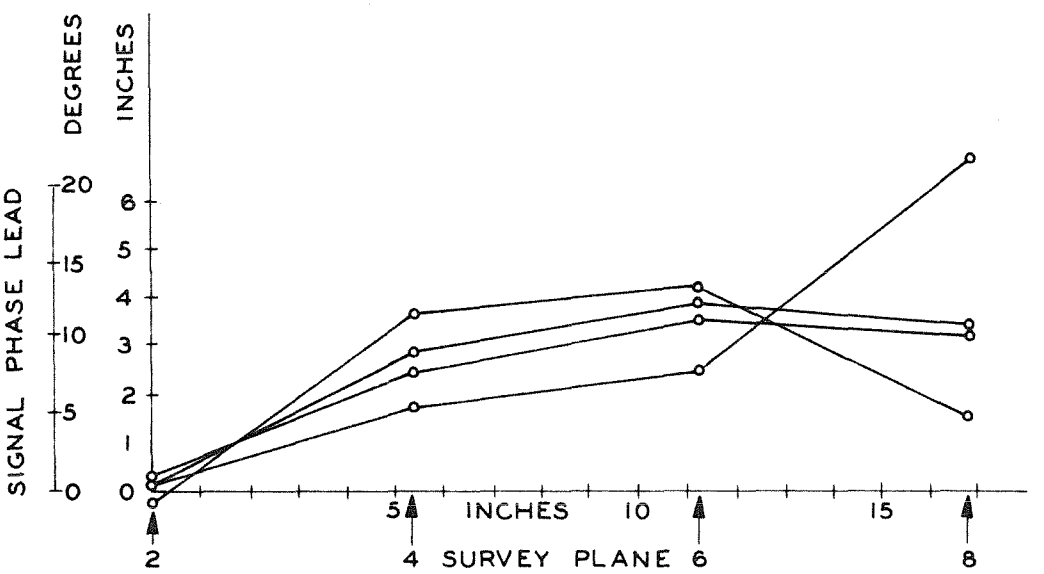

(A) PARTIAL STALL

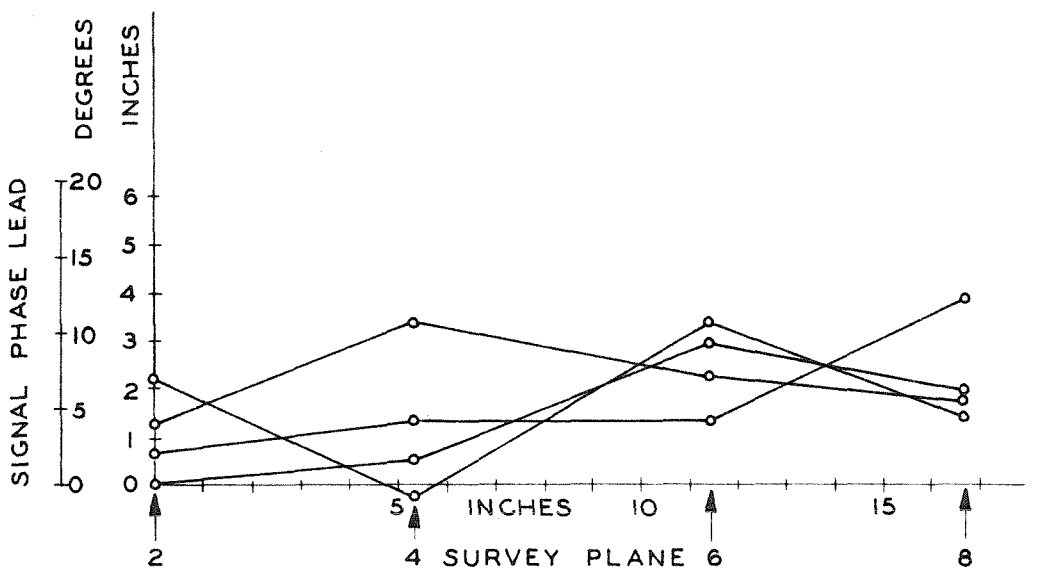

(B) FULL STALL

FIG. 17 SIGNAL PHASE RELATIONSHIPS, THREE-STAGE, FREE-VORTEX BLADES

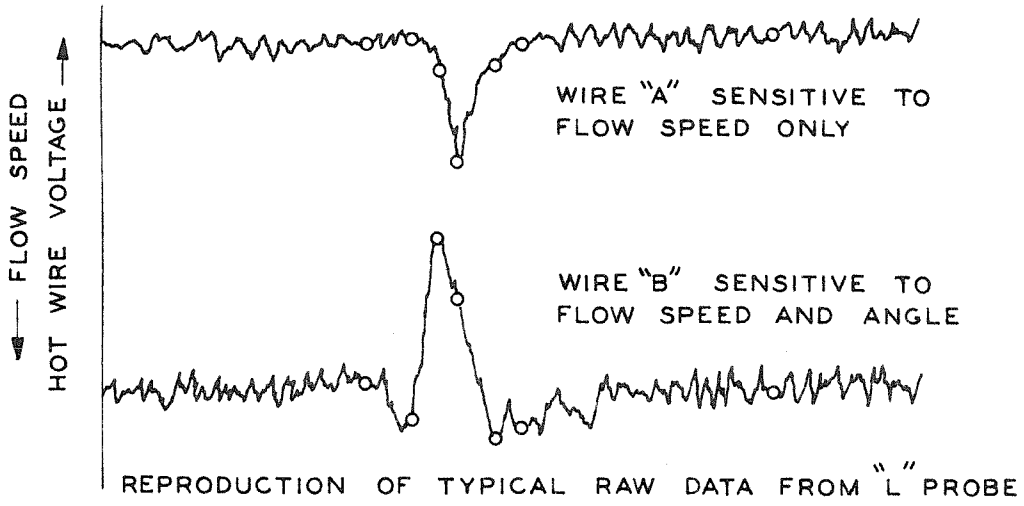

REPRODUCTION OF TYPICAL RAW DATA FROM "L" PROBE

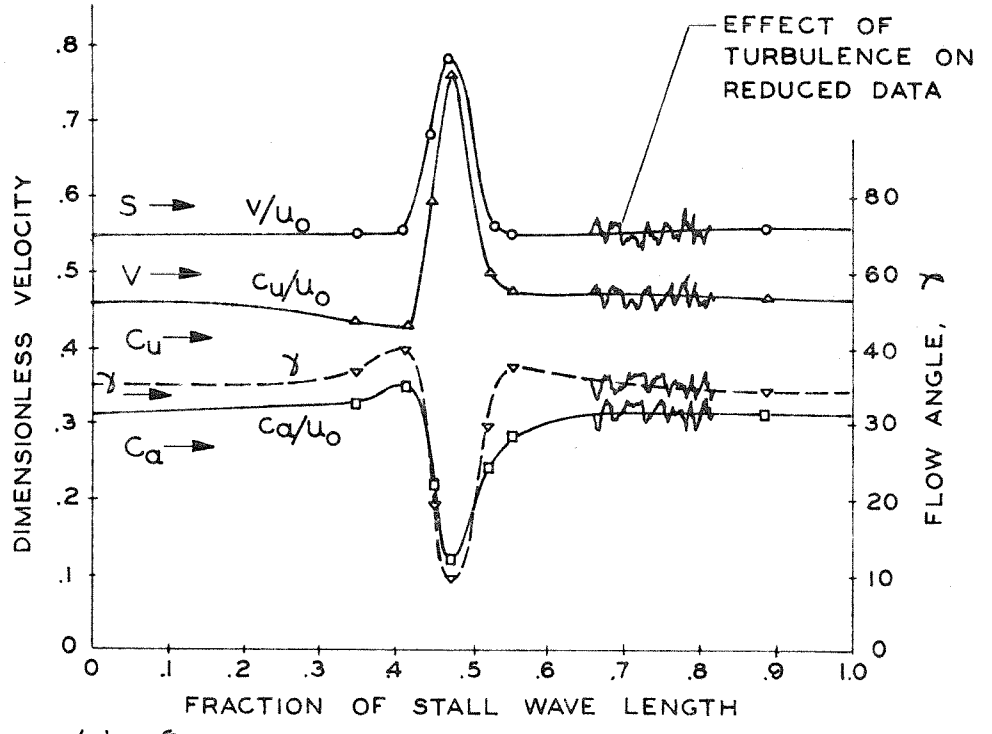

(A) $\bar{\xi} = 0.95$ BLADING: FREE VORTEX, $V_1 - R_2 - S_3$ $V_2 V_3$

SURVEY PLANE

LEGEND FOR FIG.

$V \rightarrow = V/u_o$

$C_u \rightarrow = C_u/u_o$

$C_a \rightarrow = C_a/u_o$

$\gamma \rightarrow = \gamma$

} DATA FOR UNSTALLED FLOW WITH STALL IMMINENT

$S \rightarrow$ = LOCAL STALL PROPAGATION VELOCITY

FIG. 18 VELOCITY DISTRIBUTION BEHIND FREE VORTEX ROTOR DURING PARTIAL STALL

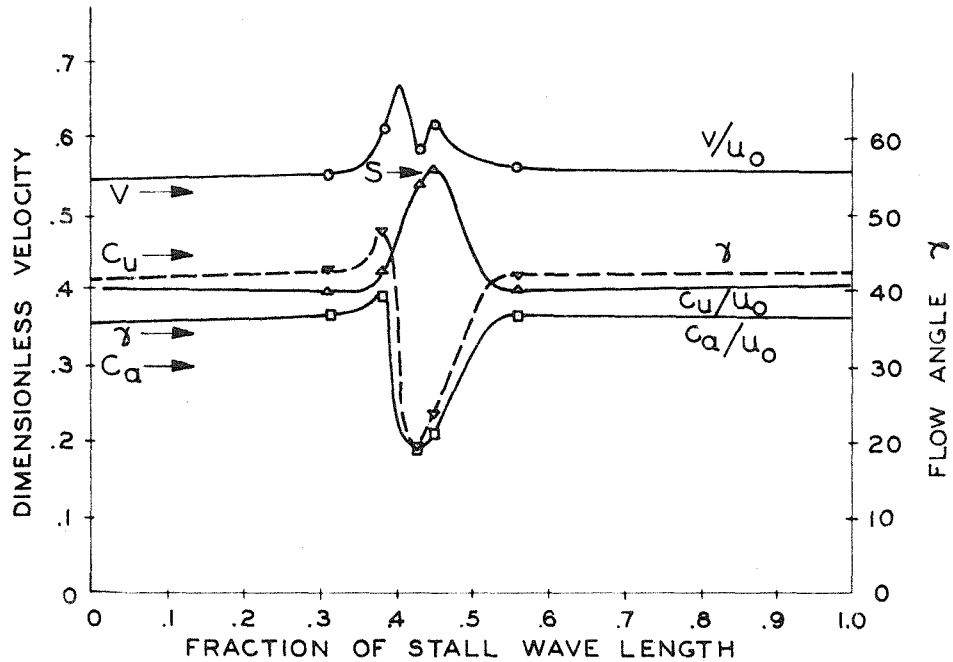

(B) $\xi = 0.90$

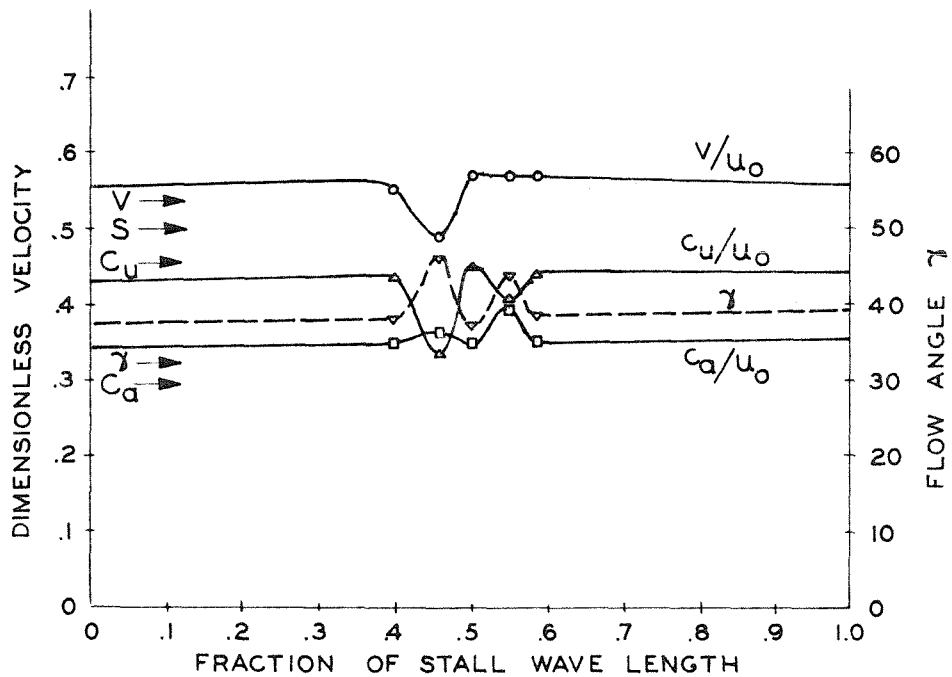

(C) $\xi = 0.80$ BLADING: FREE VORTEX, $V_1 - - R_2 - - S_3\ V_2 V_3$

SURVEY PLANE

FIG. 18 (CONTINUED)

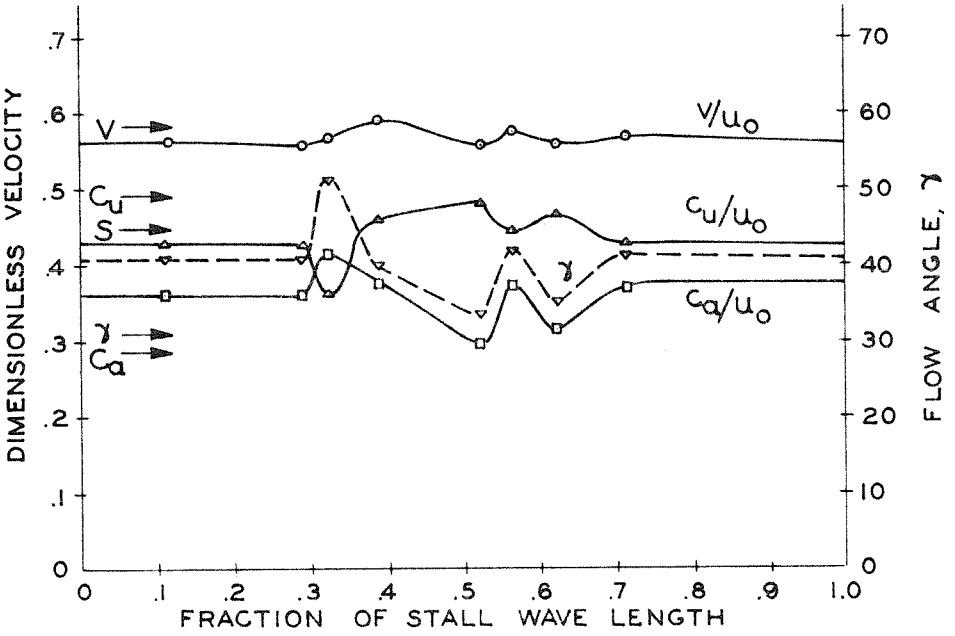

(D) ξ = 0.70

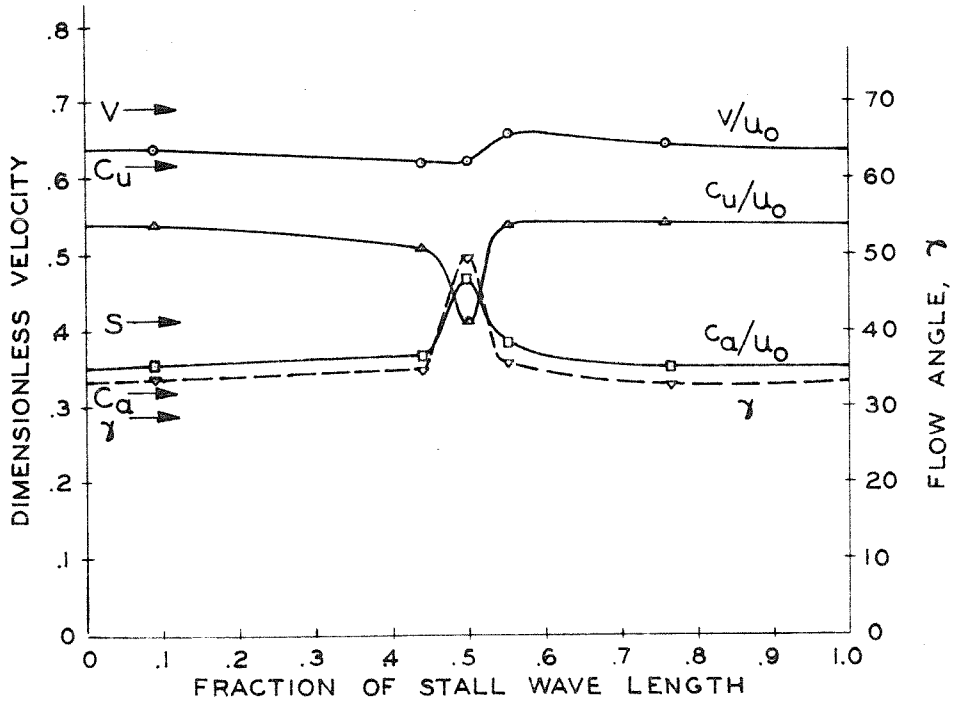

(E) ξ = 0.65 BLADING: FREE VORTEX, V_1 --R_2--S_3 V_2 V_3

└ SURVEY PLANE

FIG. 18 (CONCLUDED)

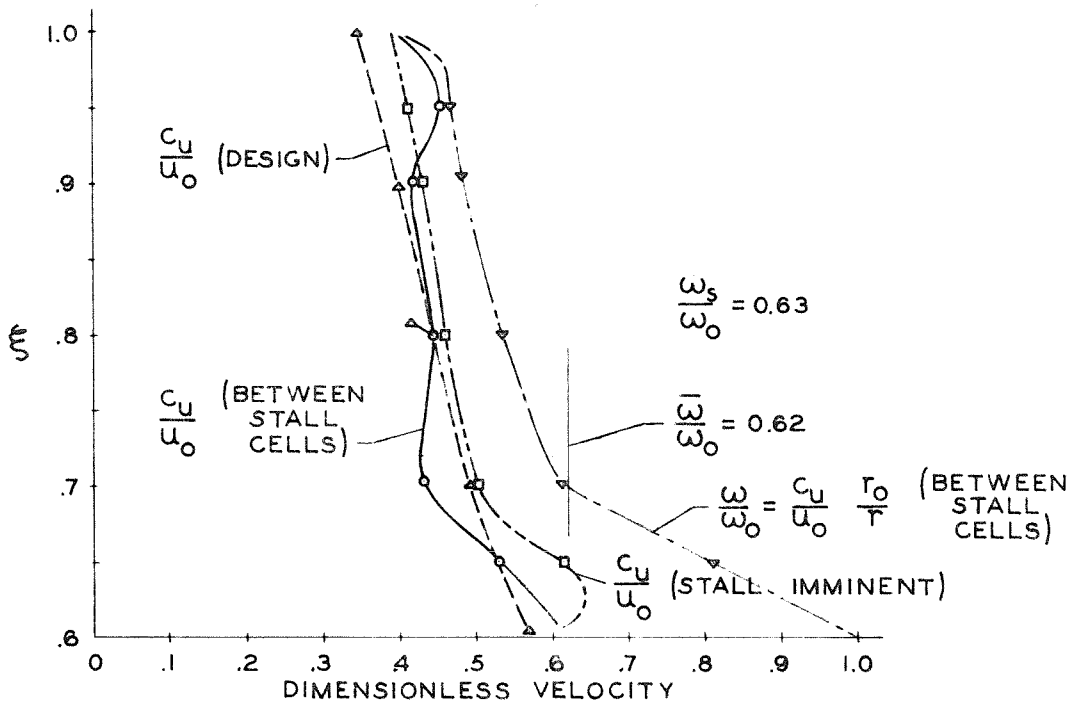

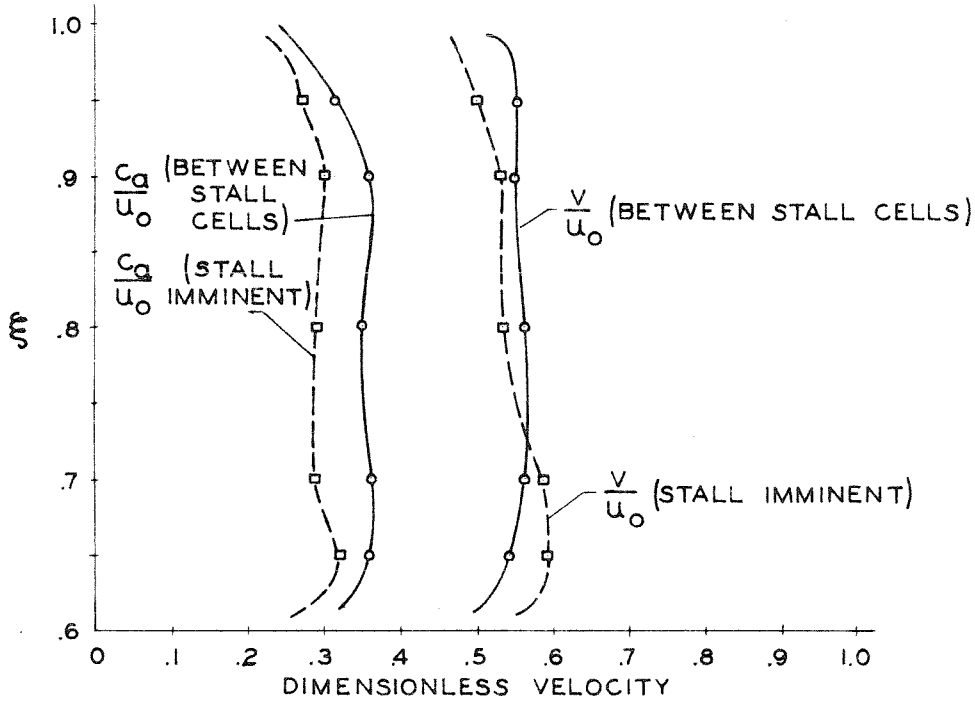

BLADING: FREE VORTEX, $V_1 - R_2 - S_3 \; V_2 V_3$

FIG. 19 RADIAL DISTRIBUTION OF FLOW COMPONENTS BEHIND ROTOR BEFORE AND DURING PARTIAL STALL PROPAGATION

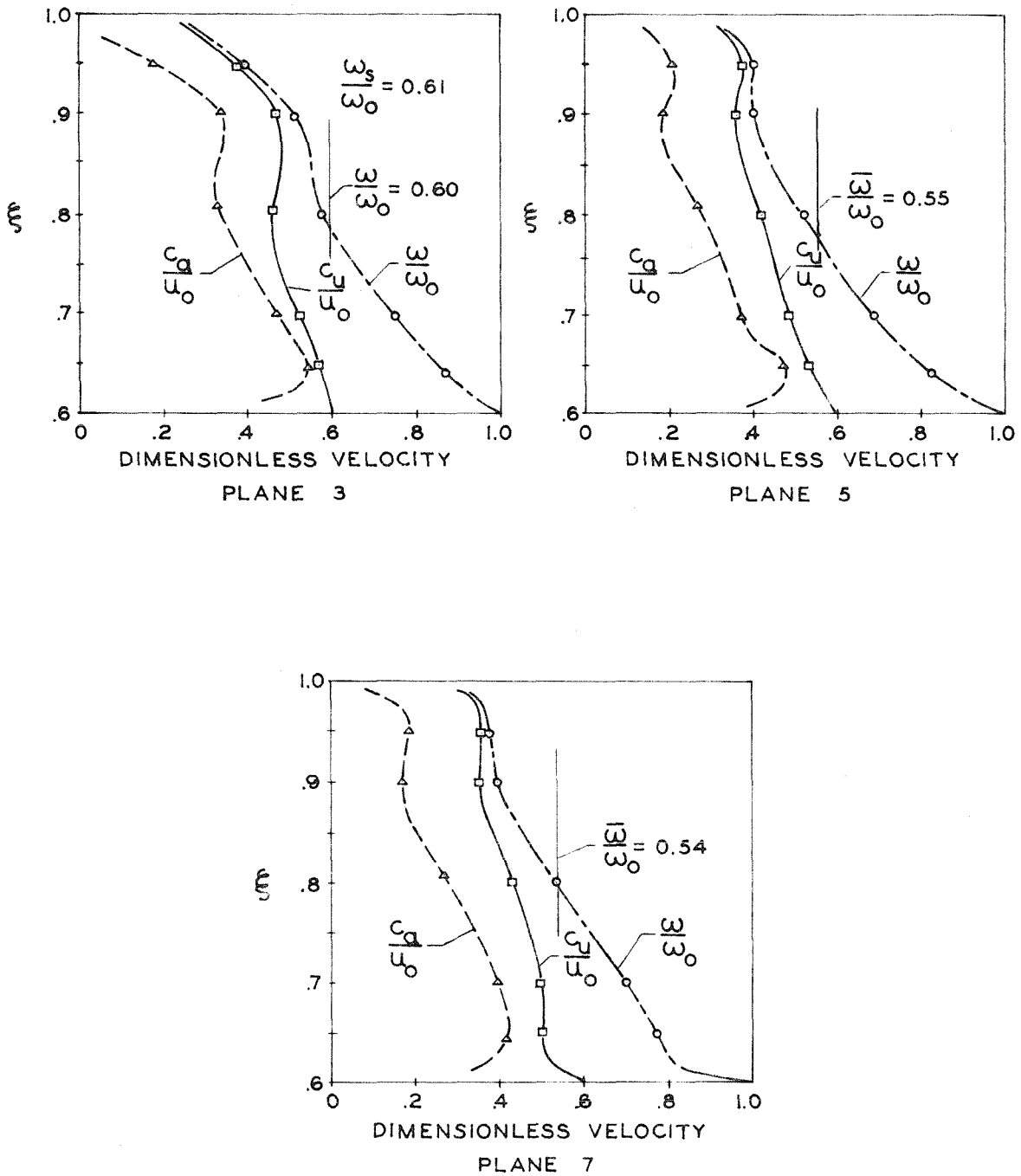

FIG. 20 AXIAL VARIATION OF RADIAL DISTRIBUTION OF FLOW COMPONENTS DURING PARTIAL STALL PROPAGATION

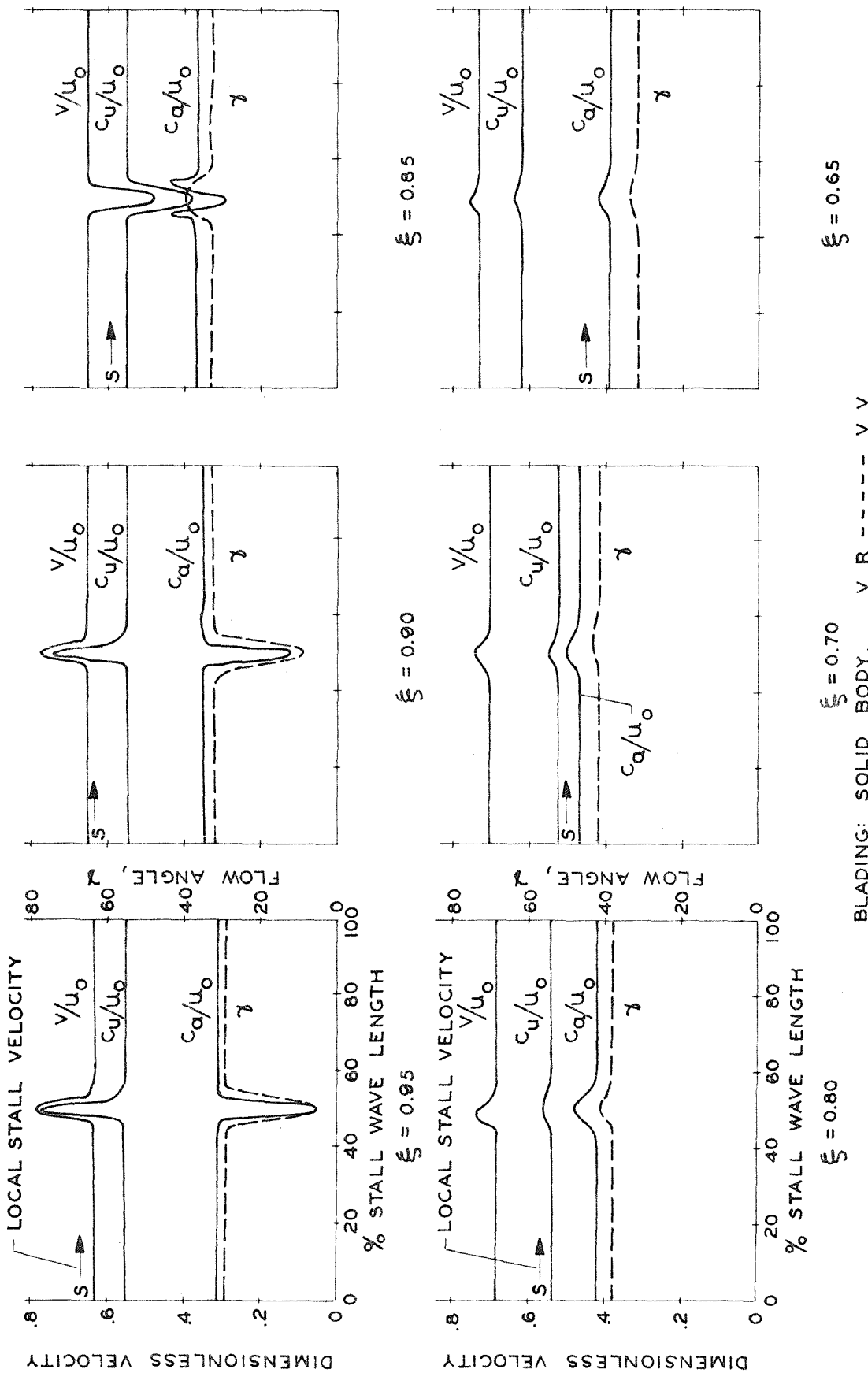

FIG. 21 VELOCITY DISTRIBUTION BEHIND SOLID BODY ROTOR DURING PARTIAL STALL

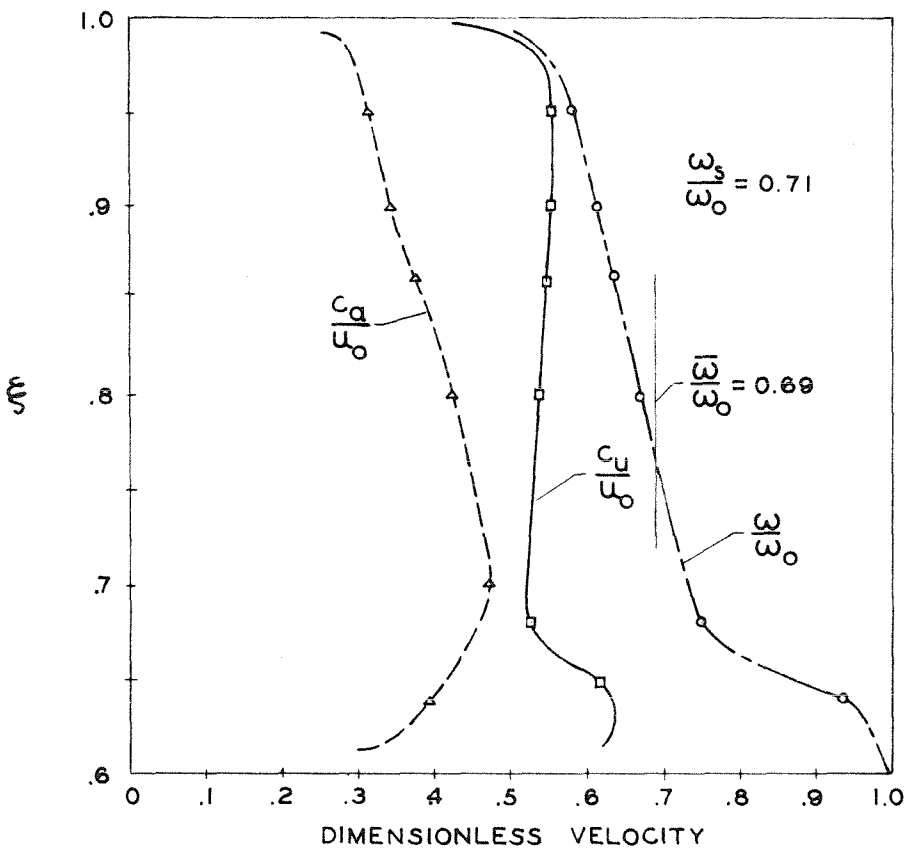

BLADING: SOLID BODY, $V_1 R_1$ ----- $V_2 V_3$

FIG. 22 RADIAL DISTRIBUTION OF VELOCITY COMPONENTS BETWEEN PARTIAL STALL CELLS BEHIND SOLID-BODY ROTOR

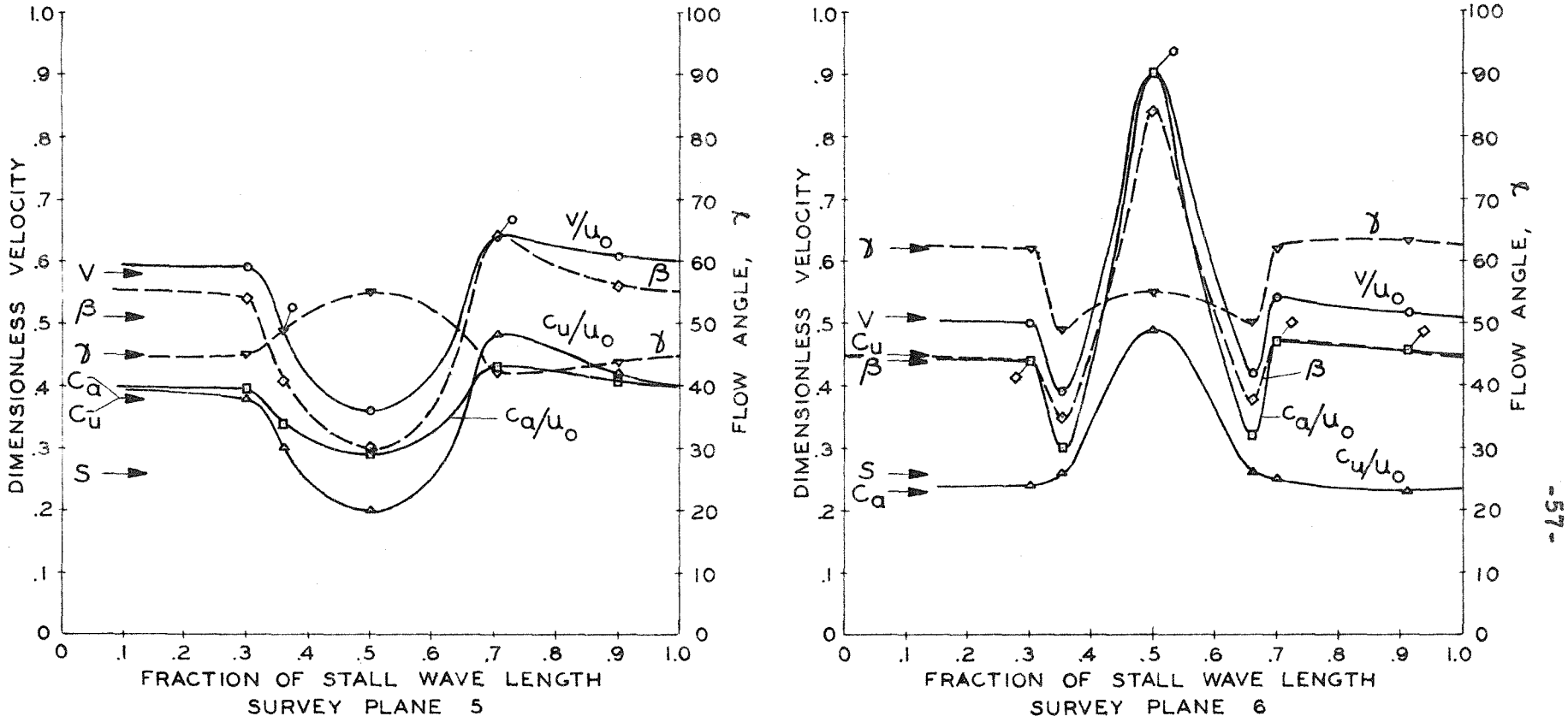

ξ = 0.69 BLADING: FREE VORTEX, V R S R S R S V V
1 1 1 2 2 3 3 2 3

5 6 SURVEY PLANES

FLOW COMPONENTS WITH STALL IMMINENT: V → C_a → C_u → β → γ →

LOCAL STALL SPEED: S →

FIG. 23 VELOCITY DISTRIBUTION ON THREE STAGE, FREE-VORTEX BLADES DURING PARTIAL STALL

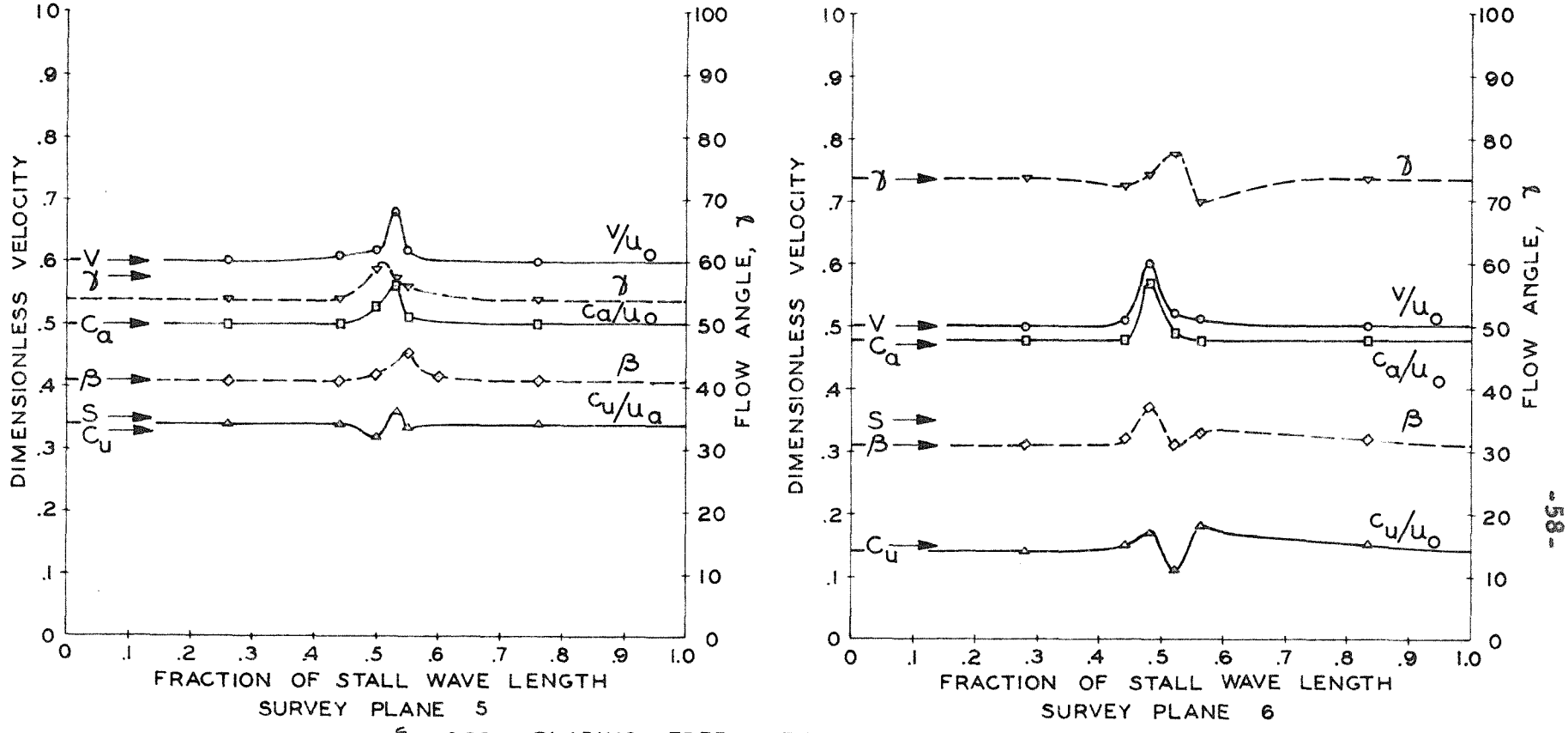

ξ = 0.92 BLADING: FREE VORTEX, $V_1 R_1 S_1 R_2 S_2 R_3 S_3 V_2 V_3$

5 6 SURVEY PLANES

FLOW COMPONENTS WITH STALL IMMINENT: $V \rightarrow C_a \rightarrow C_u \rightarrow \beta \rightarrow \gamma \rightarrow$

LOCAL STALL SPEED: $S \rightarrow$

FIG. 23 (CONTINUED)

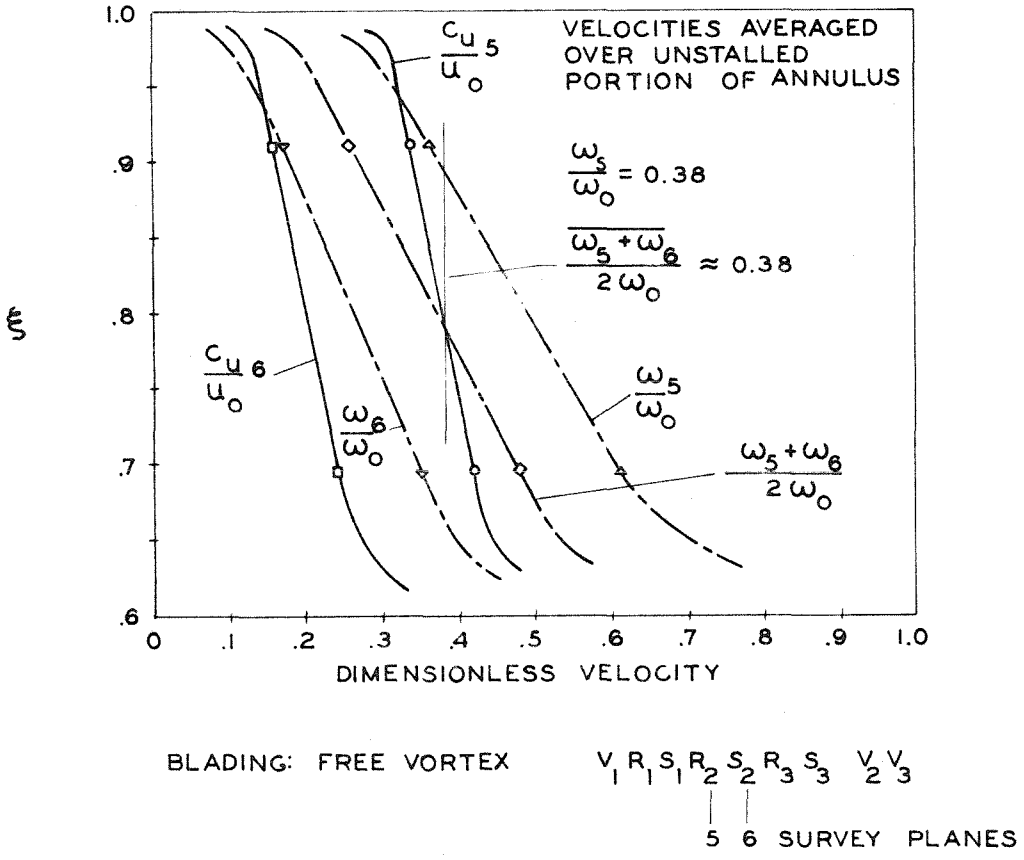

FIG. 24 RADIAL DISTRIBUTION OF WHIRL VELOCITY BETWEEN PARTIAL STALL CELLS ON THREE STAGE, FREE-VORTEX BLADES

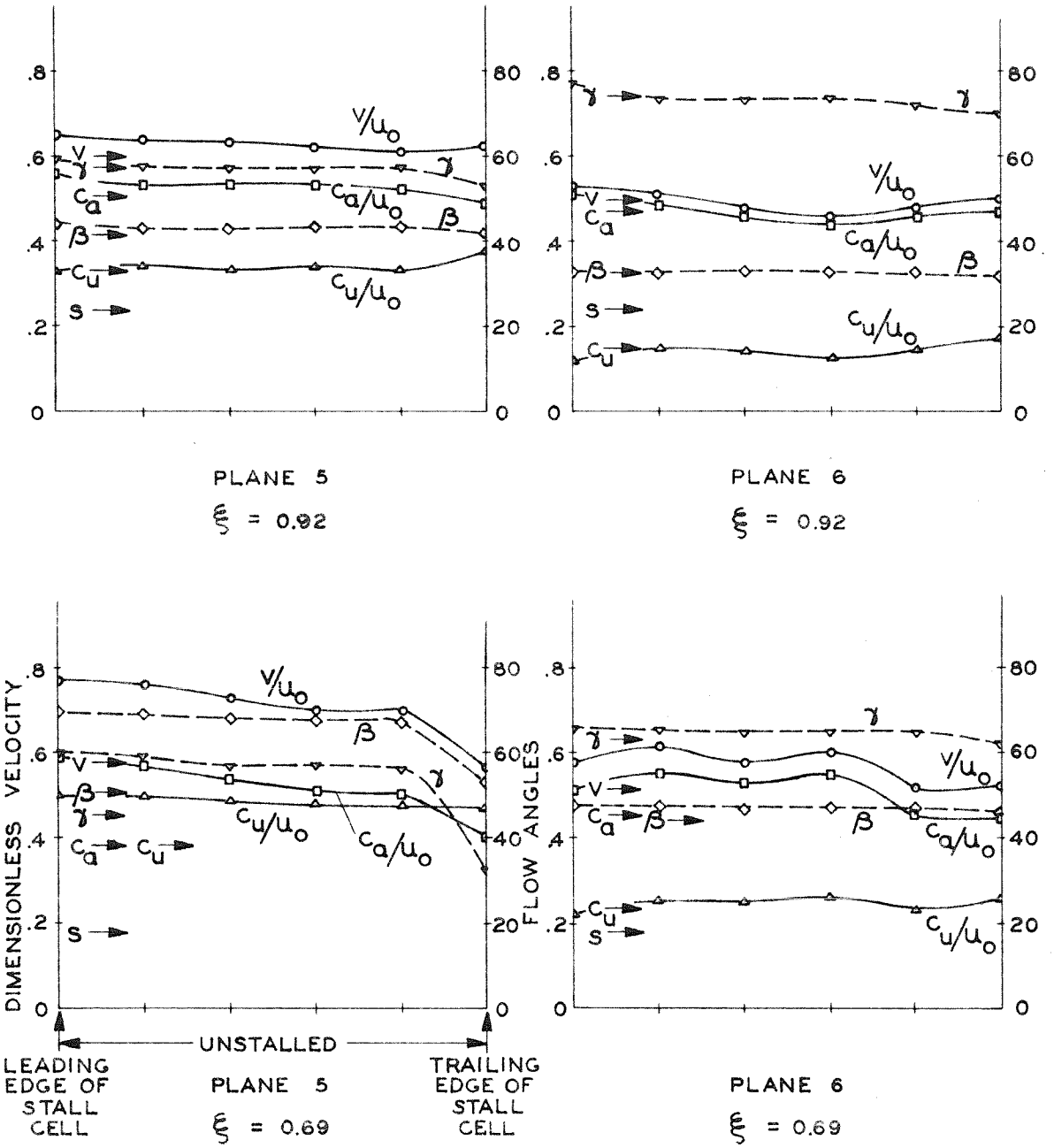

FIG. 25 VELOCITY COMPONENTS BETWEEN PASSAGES OF FULL STALL CELL ON THREE-STAGE FREE VORTEX BLADES

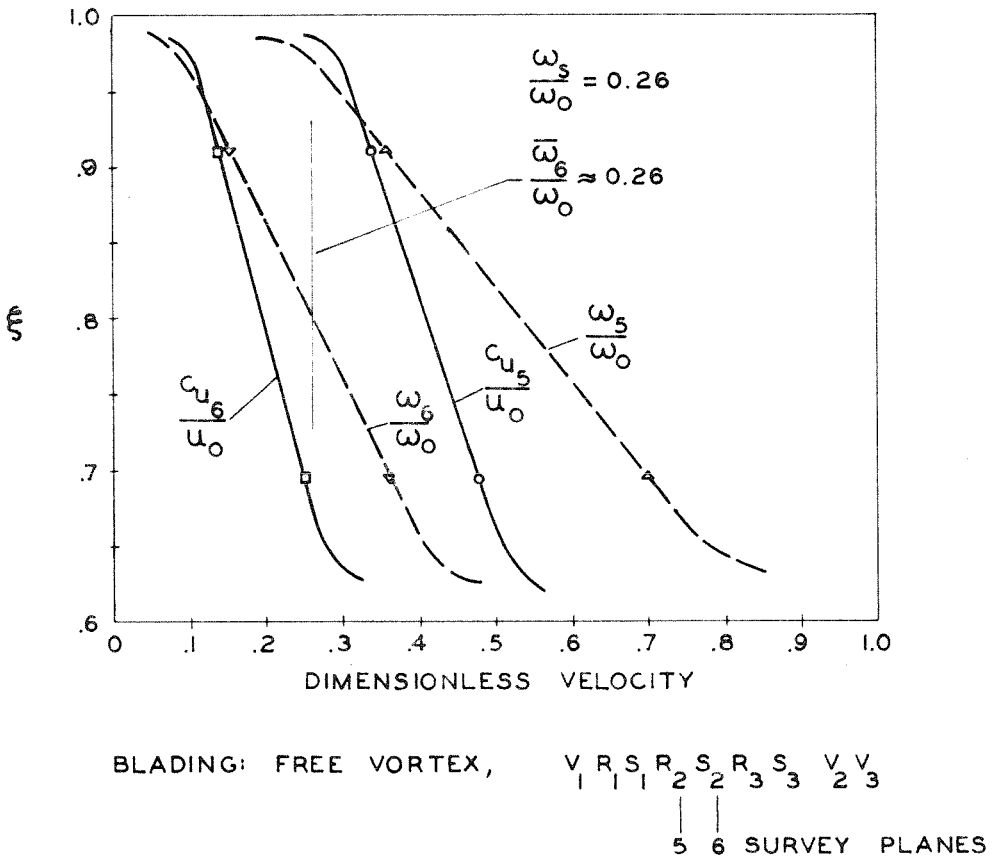

FIG. 26 RADIAL DISTRIBUTION OF WHIRL VELOCITY BETWEEN PASSAGES OF FULL STALL CELL ON THREE-STAGE, FREE VORTEX BLADES

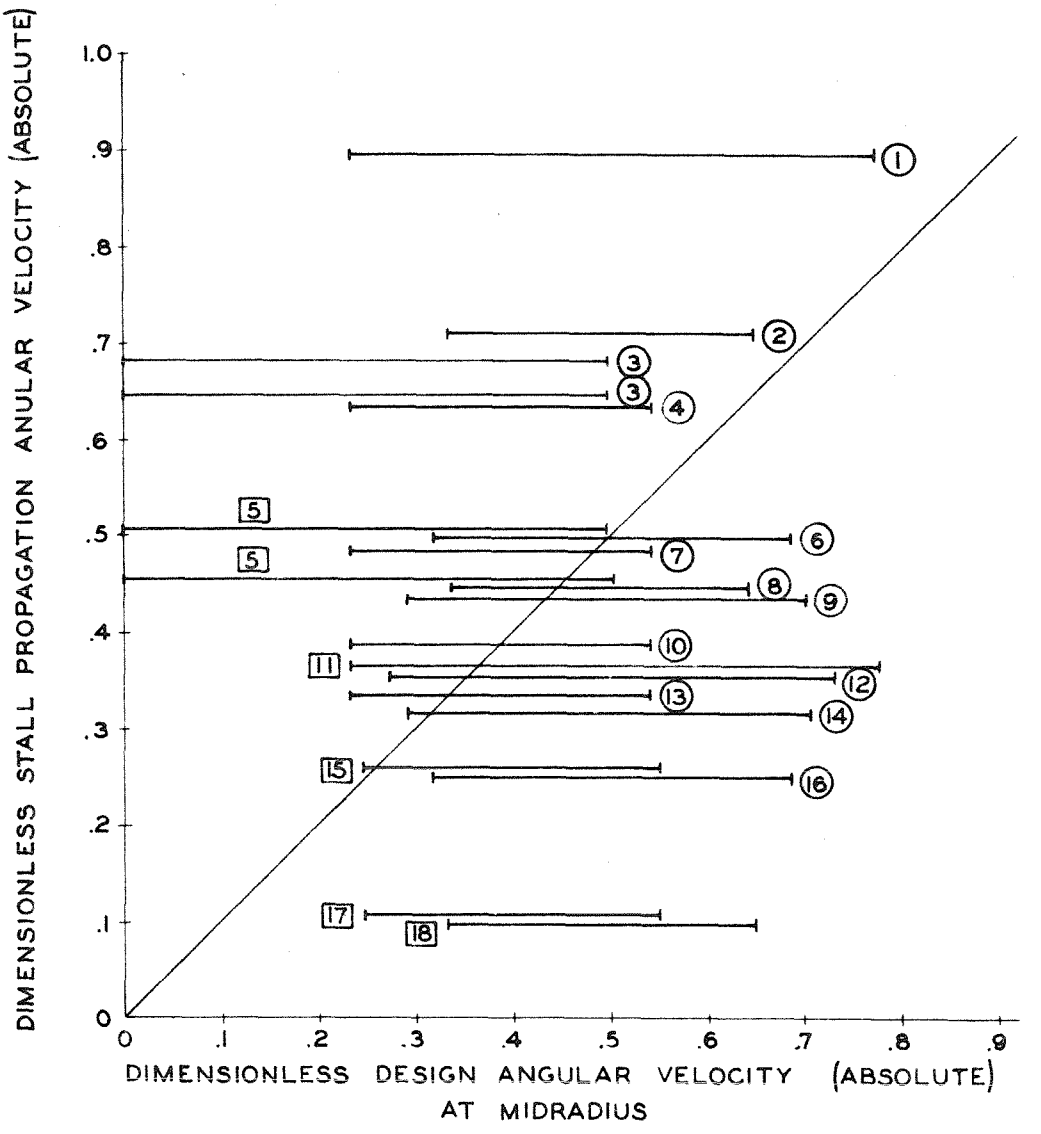

CASE	REFERENCE	STAGES	CASE	REFERENCE	STAGES
1	20	1	10	5	3
2	THIS PAPER	(ROTOR)	11	20	1
3	21	(ROTOR)	12	23	1 & 2
4	THIS PAPER	(SEPARATED)	13	THIS PAPER	1 *
5	21	(ROTOR)	14	20	1
6	24	1	15	5	3
7	5	1	16	24	1
8	5	1	17	5	1
9	22	1	18	5	1

* SEPARATED, STALL TRAVELS ON STATOR

FIG. 27 COMPARISON OF STALL PROPAGATION VELOCITIES WITH DESIGN FLOW VELOCITIES